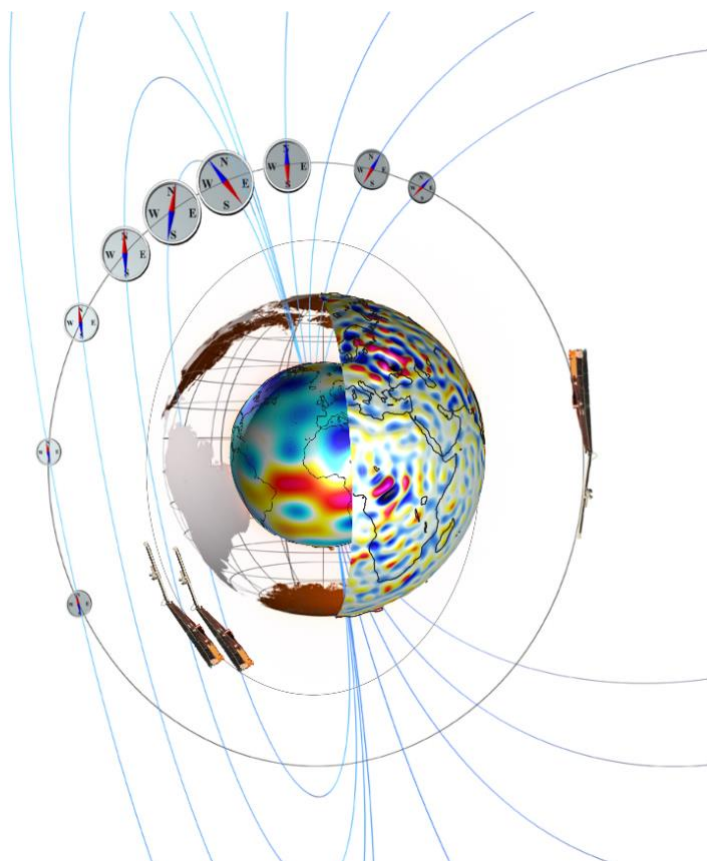

Data, Innovation, and Science Cluster

Swarm-TIRO Validation Report



Doc. no: SW-DS-GFZ-GS-013, Rev: 1, 17 May 2022

Prepared:

Lucas Schreiter

Date 17 May 2022

Scientist

Checked:

Guram Kervalishvili

Date 17 May 2022

GFZ Team Leader

Approved:

Claudia Stolle

Date 17 May 2022

TIRO Project Leader

© GFZ, Germany, 2022. Proprietary and intellectual rights of GFZ, Germany are involved in the subject-matter of this material and all manufacturing, reproduction, use, disclosure, and sales rights pertaining to such subject-matter are expressly reserved. This material is submitted for a specific purpose as agreed in writing, and the recipient by accepting this material agrees that this material will not be used, copied, or reproduced in whole or in part nor its contents (or any part thereof) revealed in any manner or to any third party, except own staff, to meet the purpose for which it was submitted and subject to the terms of the written agreement.

Record of Changes

Reason	Description	Rev	Date
Initial vers.	Released.	1 dA	11 Apr 2022
Email from Klaus to Guram: 09.05.2022 08h51	Text and figure caption updates according to feedback after the final presentation.	1 dB	12 May 2022
Signature		1	17 May 2022

Table of Contents

1	Introduction.....	8
1.1	Scope and applicability.....	8
2	Applicable and Reference Documentation	8
2.1	Applicable Documents	8
2.2	Reference Documents.....	8
2.3	Abbreviations	9
3	Analysis and Validation	11
3.1	Total Electron Content (TEC).....	11
3.1.1	Mathematical description	12
3.1.2	Observations in RINEX – Observations in TEC file.....	12
3.1.3	Consistency check	14
3.1.4	Intersatellite comparisons during conjunctions	16
3.1.4.1	CHAMP and GRACE	16
3.1.4.2	GRACE and GOCE	17
3.1.4.3	GRACE and Swarm	18
3.1.4.4	Swarm and GRACE-FO	21
3.2	K-Band ranging (KBR) electron density	24
3.2.1	Validation with radar observations.....	25
3.2.2	Swarm B and GRACE-FO conjunctions	30
3.2.3	Climatology	31
4	Summary and conclusions	33

List of Figures

Figure 3.1-1. CHAMP: Ratio of observations used in the final TEC product compared to full observation sets in the RINEX files. Single PRN are plotted in coloured points, whereas the black dots indicate the mean.	13
Figure 3.1-2. Same as Figure 3.1-1 but for GRACE A (left) and GRACE B (right).....	13
Figure 3.1-3. Same as Figure 3.1-1 but for GRACE-FO 1 (left) and GRACE-FO 2 (right).....	13
Figure 3.1-4. Full observation sets in the RINEX files for GRACE-FO 1 (left) and GRACE-FO 2(right)....	14
Figure 3.1-5. Minimum and maximum daily vertical mapped TEC values for CHAMP (left) and receiver P1-P2 DCB estimates in TECU (right).....	15
Figure 3.1-6. Same as Figure 3.1-5 but for GRACE.....	15
Figure 3.1-7. Same as Figure 3.1-5 but for GRACE-FO.....	15

Figure 3.1-8. Distribution of CHAMP and GRACE (A top, B bottom) conjunctions in geographic and geomagnetic co-ordinates. 17

Figure 3.1-9. Histogram of TEC differences at conjunction points for CHAMP and GRACE. Blue: without IRI compensation of TEC and orange: with IRI TEC compensation. 17

Figure 3.1-10. Distribution of GOCE and GRACE (A top, B bottom) conjunctions in geographical and geomagnetic co-ordinates. 18

Figure 3.1-11. Histogram of TEC differences at conjunction points for GOCE and GRACE. Blue: without IRI compensation of TEC and orange: with IRI TEC compensation. 18

Figure 3.1-12. Distribution of Swarm A and GRACE (A top, B bottom) conjunctions in geographical and geomagnetic coordinates. 19

Figure 3.1-13. Histogram of TEC differences at conjunction points for Swarm A and GRACE. Blue: without IRI compensation of TEC and orange: with IRI TEC compensation. 19

Figure 3.1-14. Distribution of Swarm B and GRACE (A top, B bottom) conjunctions in geographical and geomagnetic coordinates. 20

Figure 3.1-15. Histogram of TEC differences at conjunction points for Swarm B and GRACE. Blue: without IRI compensation of TEC and orange: with IRI TEC compensation. 20

Figure 3.1-16. Distribution of Swarm C and GRACE (A top, B bottom) conjunctions in geographical and geomagnetic coordinates. 21

Figure 3.1-17. Histogram of TEC differences at conjunction points for Swarm C and GRACE. Blue: without IRI compensation of TEC and orange: with IRI TEC compensation. 21

Figure 3.1-18. Distribution of Swarm A and GRACE-FO (1 top, 2 bottom) conjunctions in geographical and geomagnetic coordinates. 22

Figure 3.1-19. Histogram of TEC differences at conjunction points for Swarm A and GRACE-FO. Blue: without IRI compensation of TEC and orange: with IRI TEC compensation. 22

Figure 3.1-20. Distribution of Swarm B and GRACE-FO (1 top, 2 bottom) conjunctions in geographical and geomagnetic coordinates. 23

Figure 3.1-21. Histogram of TEC differences at conjunction points for Swarm B and GRACE-FO. Blue: without IRI compensation of TEC and orange: with IRI TEC compensation. 23

Figure 3.1-22. Distribution of Swarm C and GRACE-FO (1 top, 2 bottom) conjunctions in geographical and geomagnetic coordinates. 24

Figure 3.1-23. Histogram of TEC differences at conjunction points for Swarm C and GRACE-FO. Blue: without IRI compensation of TEC and orange: with IRI TEC compensation. 24

Figure 3.2-1. Mean electron density observed by GRACE (red) and GRACE-FO KBR (blue) compared to the F10.7 solar flux index. 25

Figure 3.2-2. Radar stations used for validation of the KBR derived electron density. 25

Figure 3.2-3. Calibration differences to radar stations for GRACE. And the correlation between Radar values and the IRI calibrated electron density. 28

Figure 3.2-4. Calibration differences to radar stations for GRACE-FO. 29

Figure 3.2-5. Radar calibration offsets compared to the F10.7 Index. 30

Figure 3.2-6. Histogram of electron density differences at conjunctions between Swarm B and GRACE-FO (left), and scatter plot to compare the differences in electron density to the altitude difference. Colour coding is used to indicate the dependency on magnetic latitude. 30

Figure 3.2-7. Mean and standard deviation of GRACE electron density binned in magnetic latitude (2°) and magnetic local time (30 minutes). The solar maximum year 2003 and the solar minimum year 2008 are displayed. 31

Figure 3.2-8. Mean and standard deviation of GRACE-FO electron density binned in magnetic latitude (2°) and magnetic local time (30 minutes). The years 2019 and 2020 are displayed..... 32

1 Introduction

1.1 Scope and applicability

This document comprises the summary and main results of the validation activity of Swarm-TIRO Level 2 (L2) products in response to the requirements of [AD-1]. Swarm-TIRO includes two groups of products: Total Electron Content (TEC) derived from the dual frequency Global Positioning System (GPS) observations and electron density (NE) derived from the dual frequency measurements obtained from the inter-satellite K-Band ranging (KBR) system using measurements from the following multi-satellite missions [AD-2]:

- CHAMP – TEC_TMS_2F;
- GRACE – TEC1TMS_2F, TEC2TMS_2F, and NE__KBR_2F;
- GRACE-FO – TEC1TMS_2F, TEC2TMS_2F, and NE__KBR_2F.

Current or updated version of this document is available in the SVN folder: https://smart-svn.spacecenter.dk/svn/smart/SwarmDISC/DISC_Projects/ITT3_3_TIRO/Deliverables/.

The Swarm-TIRO Product Definition Document (PDD) [AD-2] is available in the SVN folder: https://smart-svn.spacecenter.dk/svn/smart/SwarmDISC/DISC_Projects/ITT3_3_TIRO/Deliverables/TIRO.

2 Applicable and Reference Documentation

2.1 Applicable Documents

The following documents are applicable to the definitions within this document.

- [AD-1] SW-OF-GFZ-GS-126_3-3_TIRO, Proposal for Swarm DISC ITT 3.3, Swarm-TIRO – Topside Ionosphere Radio Observations from multiple LEO-missions.
- [AD-2] SW-DS-GFZ-GS-010_3-3_TIRO_PDD, Product Definition Document.
- [AD-3] SW-TR-GFZ-GS-0007, Swarm L2 TEC Product Description.
- [AD-4] GO-TN-HPF-GS-0337, Computation of TEC and Rate of TEC Index (ROTI) from GOCE GPS.
- [AD-5] SW-DS-GFZ-GS-012_3-3_TIRO_DPA, Description of the Processing Algorithms.
- [AD-6] SW-DS-GFZ-GS-0004, Swarm Level 2 Processing System – GFZ Detailed Processing Model TEC.

2.2 Reference Documents

- [RD-1] Bilitza, D., Altadill, D., Truhlik, V., Shubin, V., Galkin, I., Reinisch, B., Huang, X. (2017), International Reference Ionosphere 2016: From ionospheric climate to real-time weather predictions, Space Weather, 15, 418– 429, doi: [10.1002/2016SW001593](https://doi.org/10.1002/2016SW001593).
- [RD-2] Blewitt, G. (1990), An automated editing algorithm for GPS data, Geophysical Research Letters, 17, 199–202, doi: [10.1029/GL017i003p00199](https://doi.org/10.1029/GL017i003p00199).
- [RD-3] Yue, X., Schreiner, W. S., Hunt, D. C., Rocken, C., Kuo, Y.-H. (2011), Quantitative evaluation of the low Earth orbit satellite based slant total electron content determination, Space Weather, 9, S09001, doi: [10.1029/2011SW000687](https://doi.org/10.1029/2011SW000687).
- [RD-4] Noja, M., Stolle, C., Park, J., Lühr (2013), Long-term analysis of ionospheric polar patches based on CHAMP TEC data, Radio Sci., 48, 289–301, doi: [10.1002/rds.20033](https://doi.org/10.1002/rds.20033).

- [RD-5] Montenbruck, O., Kroes, R. (2003), In-flight performance analysis of the CHAMP BlackJack GPS Receiver. *GPS Solutions* **7**, 74–86, doi: [10.1007/s10291-003-0055-5](https://doi.org/10.1007/s10291-003-0055-5).
- [RD-6] The New Flex Power Mode: From GPS IIR-M and IIF Satellites with Extended Coverage Area, <https://insidegnss.com/the-new-flex-power-mode-from-gps-iir-m-and-iif-satellites-with-extended-coverage-area/>.
- [RD-7] Landerer, F., Flechtner, F., Save, H., Dahle, C. (2018). GRACE Follow-On Science Data System Newsletter Report: Oct/Nov 2018, https://www.gfz-potsdam.de/fileadmin/gfz/sec12/pdf/GRACE-FO/GRACE_FO_SDS_newsletter_No18.pdf.
- [RD-8] Nava, B., Coïsson, P., Radicella, S. M. (2008), A new version of the NeQuick ionosphere electron density model. *Journal of Atmospheric and Solar-Terrestrial Physics*, **70**(15), 1856–1862, doi: [10.1016/j.jastp.2008.01.015](https://doi.org/10.1016/j.jastp.2008.01.015).
- [RD-9] Lomidze, L., Knudsen, D. J., Burchill, J., Kouznetsov, A., & Buchert, S. C. (2018), Calibration and validation of Swarm plasma densities and electron temperatures using ground-based radars and satellite radio occultation measurements. *Radio Science*, **53**, 15–36, doi: [10.1002/2017RS006415](https://doi.org/10.1002/2017RS006415).
- [RD-10] Smirnov, A., Shprits, Y., Zhelavskaya, I., Lühr, H., Xiong, C., Goss, A., et al. (2021), Intercalibration of the plasma density measurements in Earth's topside ionosphere. *Journal of Geophysical Research: Space Physics*, **126**, e2021JA029334, doi: [10.1029/2021JA029334](https://doi.org/10.1029/2021JA029334).
- [RD-11] Xiong, C., Lühr, H., Ma, S. Y., & Schlegel, K. (2015), Validation of GRACE electron densities by incoherent scatter radar data and estimation of plasma scale height in the topside ionosphere. *Advances in Space Research*, **55**, 2048–2057, doi: [10.1016/j.asr.2014.07.022](https://doi.org/10.1016/j.asr.2014.07.022).

2.3 Abbreviations

A list of acronyms and abbreviations used by Swarm partners can be found [here](#). Any acronyms or abbreviations not found on the online list but used in this document can be found below.

Acronym or abbreviation	Description
AD	Applicable Document
CHAMP	CHALLENGING Minisatellite Payload
GOCE	Gravity field and Ocean Circulation Explorer
GRACE	Gravity Recovery and Climate Experiment
GRACE-FO	GRACE Follow-On
KBR	K-Band Ranging
NE	electron density
PRN	Pseudorandom Noise
IRI-2016	International Reference Ionosphere 2016
RD	Reference Documents

Acronym or abbreviation	Description
RINEX	Receiver Independent Exchange Format
SNR	Signal-to-Noise Ratio
sTEC	slant TEC
TEC	Total Electron Content
TECU	TEC Unit
TIRO	Topside Ionosphere Radio Observations from multiple LEO-missions
vTEC	vertical TEC

3 Analysis and Validation

The ionosphere contains ionized gas, ions and electrons. The ionization process is primarily solar-driven. Depending on solar activity, geomagnetic activity, wind systems, season, and several other drivers, the ionosphere shows a high variability from several seconds up to decades. Over the last few years, global monitoring of the ionosphere began using LEO satellites in order to access the topside parameters, which are not detectable by ground-based observation techniques, such as ground-based GPS or ionosondes. The Swarm TEC [AD-3] data set already provided valuable insight into the topside ionosphere and GOCE TEC [AD-4] provides measurements from as low as 250 km, being close to the F2 ionization peak. Swarm-TIRO is the natural extension for the already existing data sets in Swarm DISC. The processing [AD-5] is held consistent with the already existing data sets and uses several improvements in order to ensure optimum data quality. The additional satellites link the Swarm and GOCE mission and provide full coverage starting from July 2000 (CHAMP) until today (Swarm and GRACE-FO). Currently, the time series covers almost two full solar cycles, thus allowing for long-term studies and increasing the scientific output of all the satellite missions involved.

The validation strategy starts by investigating the data set for the amount of data useable for TEC computation. The data availability should be maximized, and outliers should be successfully filtered. The time series are further investigated by accessing daily minimum and maximum values. The minimum is supposed to be around 0 with a scatter stemming from levelling uncertainties. The maximum observed TEC value is dependent on altitude, the visited local times, but also on solar activity and its evaluation shall be consistent with these parameters. Furthermore, the time series of the estimated receiver-specific P1-P2 code bias for the GPS observables are analyzed for outliers, jumps, and periodic signals. After a first single satellite the consistency check, inter-satellite comparison is performed using conjunctions linking all satellite missions providing TEC included in Swarm DISC, i.e., CHAMP, GRACE, GOCE, Swarm, and GRACE-FO. The differences in the observed TEC values are evaluated. As a result of the performed validations, we will be able to conclude that Swarm-TIRO products meet the expected accuracy, only limited by the levelling uncertainties.

Electron density derived from GRACE and GRACE-FO K Band observations is validated using the IRI-2016 model [RD-1], ground-based radar observations and conjunctions with Swarm making use of electron density measurements provided by Langmuir probes. Climatological patterns of electron density for different solar Flux levels are examined.

3.1 Total Electron Content (TEC)

Total Electron Content (TEC) is a measure of the integrated ionospheric electron density between two points. In Swarm-TIRO, the GPS slant TEC is derived, which is the integrated electron density along the line of sight between a transmitter (GPS satellite) and a receiver. For Swarm-TIRO, the GPS receivers considered are carried on board LEO satellites, namely CHAMP, GRACE, and GRACE Follow On. CHAMP and GRACE were equipped with BlackJack GPS receivers, GRACE-FO carries the TriRO-GNSS receiver, which in turn has BlackJack heritage. Electrons cause a delay in code measurements and cause advances in phase measurements, and these effects are frequency dependent. Therefore, dual-frequency measurements can be utilized to mitigate the ionospheric signal content, e.g., in coordinated estimation, and, at the same time, allows an estimate of the total amount of electrons between transmitter and receiver.

3.1.1 Mathematical description

Slant TEC (sTEC) is defined as the integrated electron density along the line of sight between a radio transmitter (e.g., GPS satellite) and receiver (e.g., on board the GRACE-FO satellite). From the frequency dependent signal delays, the line-of-sight sTEC is derived by the following equation:

$$sTEC = \frac{f_1^2 f_2^2}{f_1^2 - f_2^2} \frac{L_1 - L_2}{K} + DCB_T + DCB_R + \Delta\varepsilon \quad \text{Equation 3-1}$$

where f_1 (= 1.575,42 MHz) and f_2 (= 1.227,6 MHz) are the carrier frequencies of the, here, GPS signals in units of seconds, L_1 and L_2 are carrier phase observations in units of meters, and $K \approx 40.3 \text{ m}^3 \text{ s}^{-2}$, DCB_T and DCB_R are the differential code bias of the GPS satellite and the receiver originating from the code levelling in units of m^{-2} , respectively, and $\Delta\varepsilon$ includes ambiguities, and remaining errors in units of m^{-2} . TEC is given in TECU units (TECU) and $1 \text{ TECU} = 10^{16} \text{ electrons/m}^2$. This algorithm is based on approved methods suggested originally in [RD-2] and [RD-3] that has been adapted to process signals received at LEO-satellites [AD-5]. Applying an appropriate mapping function maps the line-of-sight sTEC into vertical TEC (vTEC) and is described in [RD-4].

The algorithm applied here to derive relative and absolute sTEC and mapping it to absolute vTEC is similar to the one that is operationally applied in the processor implemented for Swarm and a detailed algorithm description is given in [AD-6].

3.1.2 Observations in RINEX – Observations in TEC file

To derive TEC from dual-frequency GPS observations the geometry-free linear combination of phase observations $L_{gf} = L_1 - L_2$ is aligned to the geometry-free linear combination of code observations $P_{gf} = P_1 - P_2$. Biases are applied or estimated and the aligned L_{gf} is scaled to obtain TEC. Code and phase observation need to be free from outliers, jumps, or other artefacts. Pre-processing and filtering aim at two objectives: First, no outlier and artefacts should remain; thus, the dataset should be as clean as possible, and secondly, a maximum amount of data should be kept. For obtaining a grip on the amount of data, that can be assumed to be clean, we count the number of complete observation sets, i.e., P_1, P_2, L_1 , and L_2 in the Receiver Independent Exchange Format (RINEX) observation file and divide the number of observations of TEC in the CDF files by that number derived from the RINEX file. The result is the ratio of observations that passed the whole screening process. This evaluation is carried out for each GPS satellite in the observation files. The results are displayed in Figure 3.1-1, Figure 3.1-2 and Figure 3.1-3 for each satellite mission respectively. Apart from GRACE B, all the satellite ratios show jumps due to different reasons. In the case of CHAMP, these jumps are related to the different versions of RINEX processor and the operational mode of the occultation antenna. The latter can cause significant variations in multipath and code noise [RD-5]. In the case of GRACE A, these jumps are also related to switching operation modes of the occultation antenna. For GRACE-FO, the first jump visible in Figure 3 is caused by Flex power mode IV, starting in Jan. 2020 [RD-6] which can cause tracking issues for the TriRO GNSS receivers. The second jump for GRACE-FO 1 near May 2021 is related to receiver updates (see Figure 3.1-4, where the absolute number of daily observations sets in the RINEX file for each PRN is shown). The elevation mask was removed, as now also satellites below 10° elevation are tracked. Low elevation observations usually suffer from a low signal-to-noise ratio (SNR). This is also the reason, why on one hand the observations in the RINEX file increase which is shown in Figure 3.1-3, but the ratio of accepted observations decreases on the other hand because observations having low SNR values are rejected during the processing.

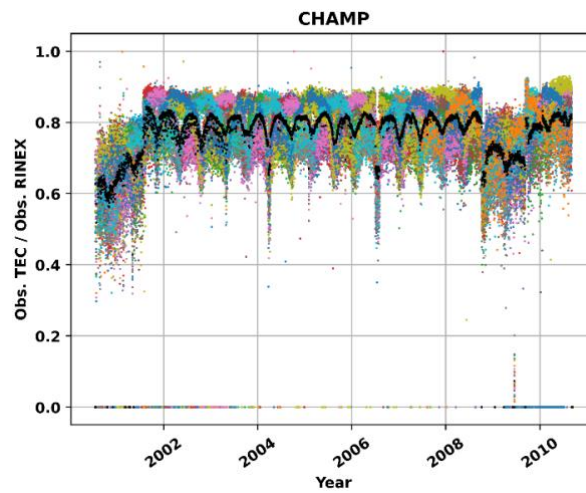


Figure 3.1-1. CHAMP: Ratio of observations used in the final TEC product compared to full observation sets in the RINEX files. Single PRN are plotted in coloured points, whereas the black dots indicate the mean.

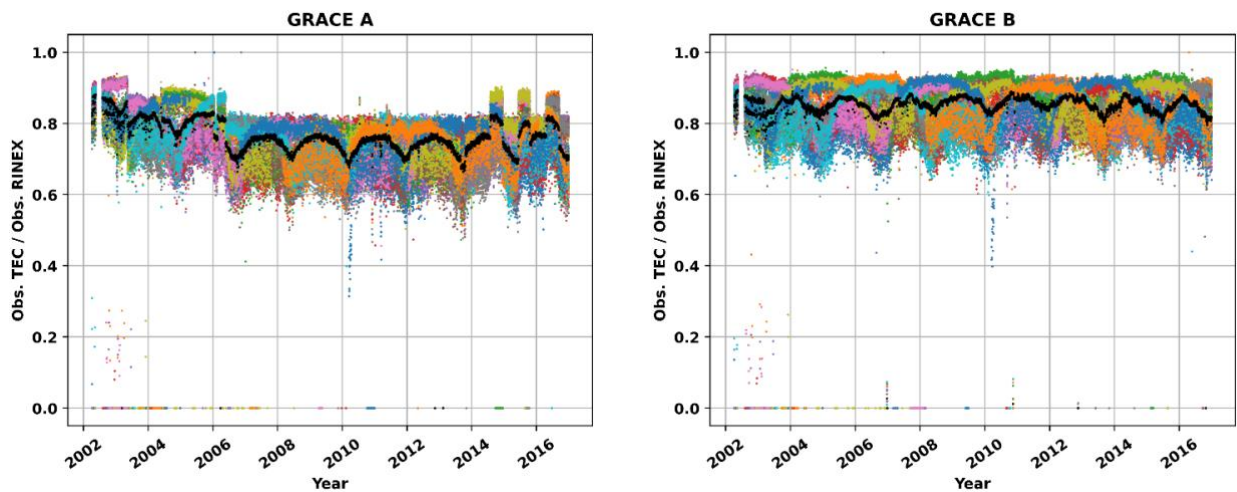


Figure 3.1-2. Same as Figure 3.1-1 but for GRACE A (left) and GRACE B (right).

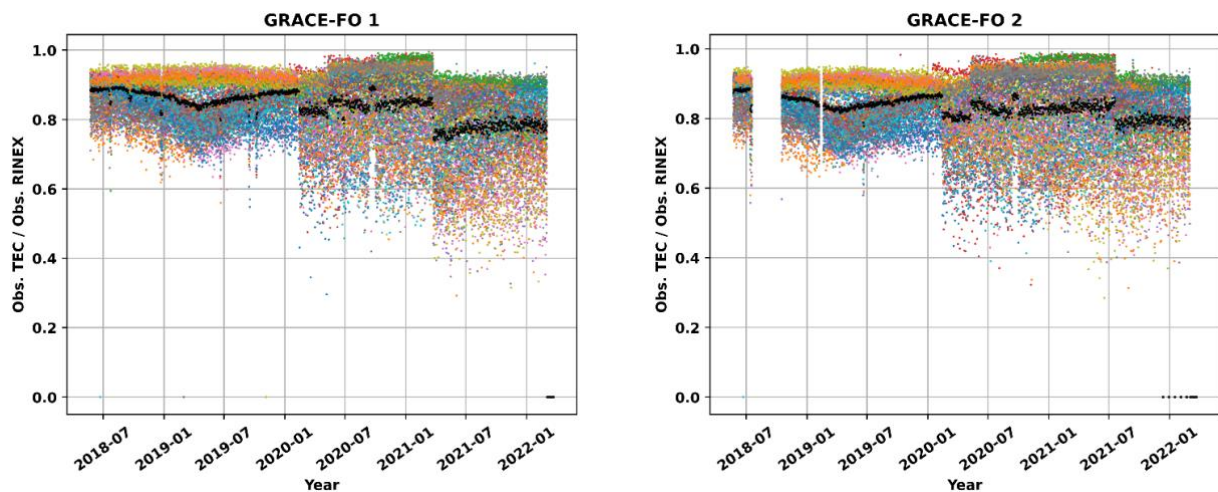


Figure 3.1-3. Same as Figure 3.1-1 but for GRACE-FO 1 (left) and GRACE-FO 2 (right).

When satellites are fully rejected for a full day (not only parts of observations), this is usually caused by the unavailable of the GPS satellite, e.g., due to satellite manoeuvres. In the case that orbits for the LEO satellite are not available, the daily CDF-output file is empty. During regular availability of GPS and LEO ephemeris, approximately 80% of the observations can be used for the TEC product. The best ratio of accepted observations is observed for GRACE-FO for the time periods, where GPS Flex power was not yet active.

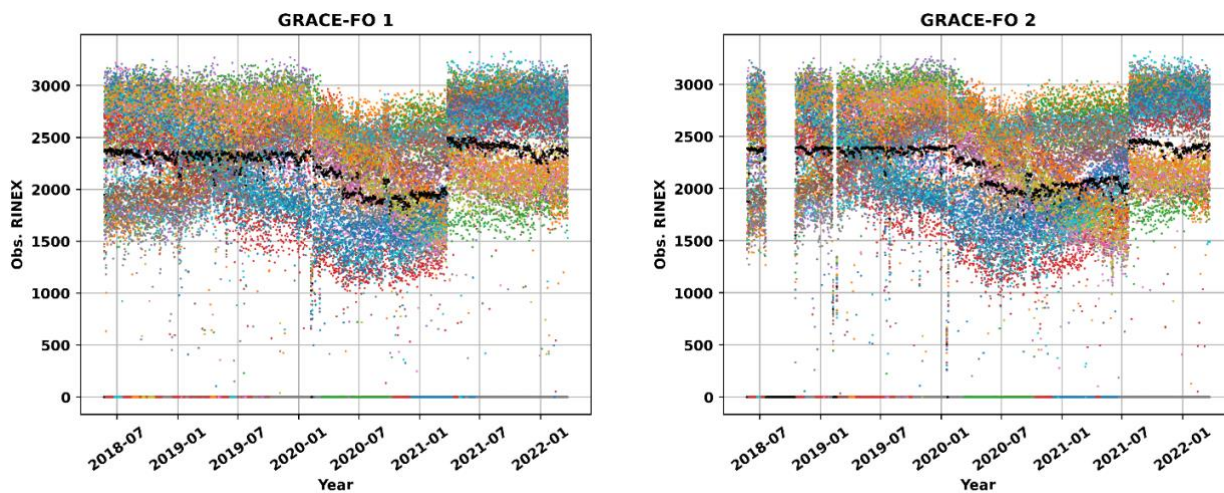


Figure 3.1-4. Full observation sets in the RINEX files for GRACE-FO 1 (left) and GRACE-FO 2(right).

3.1.3 Consistency check

For the purpose of consistency, the daily minimum and maximum vertical TEC are evaluated and screened for implausible small or large values. Due to uncertainties stemming from code levelling and receiver bias estimation negative TEC values can occur. If they do, these negative values are within the range of the levelling uncertainty of 3 TECU (see Figure 3.1-5, Figure 3.1-6, Figure 3.1-7, left, daily minimum and maximum values plotted together with the F10.7 index).

An indication of validity is similar values for flying satellite pairs, e.g., GRACE and GRACE-FO.

Another indication of validity is a positive correlation between the maximum vertical TEC value and solar activity, represented by the F10.7 index (both as 81-day mean) as a proxy. Experiments were also carried out using the daily mean TEC, which led to identical conclusions. The correlation coefficients are 0.93 for CHAMP 0.81/0.82, for GRACE A and GRACE B 0.74/0.71 for GRACE-FO 1 and GRACE-FO 2. The low correlations for GRACE-FO are caused by the solar min period with not too much variation in the F10.7 index and only little variation in the vertical TEC. On top of the vertical TEC is to a large extent determined by the different magnetic local times and altitude. An oscillation with a period of four months is visible, which coincides with the drift in local time. Furthermore, the maximum value of GRACE-FO 1 seems to be noisier than for GRACE-FO 2. That is likely caused by the occultation antenna causing additional code noise, which is active on GRACE-FO 1, but not on GRACE-FO 2.

A second consistency check is the day-to-day variation of the estimated receiver-specific P1-P2 differential code bias (see Figure 3.1-5, Figure 3.1-6, Figure 3.1-7, right). The accuracy of the estimated DCB can be expected around 1 TECU. Large inter-day variations are not expected. For CHAMP, only a few outliers exist, which are caused by numerical instabilities of the estimation. In these cases, an insufficient number of observations were found for the receiver bias estimation. Oscillations in the receiver specific P1-P2 bias in the

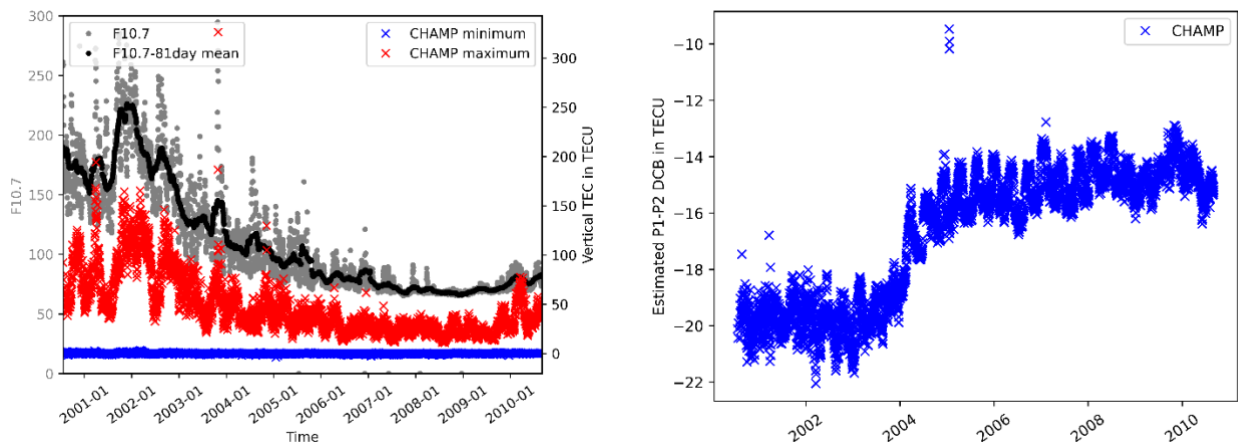


Figure 3.1-5. Minimum and maximum daily vertical mapped TEC values for CHAMP (left) and receiver P1-P2 DCB estimates in TECU (right).

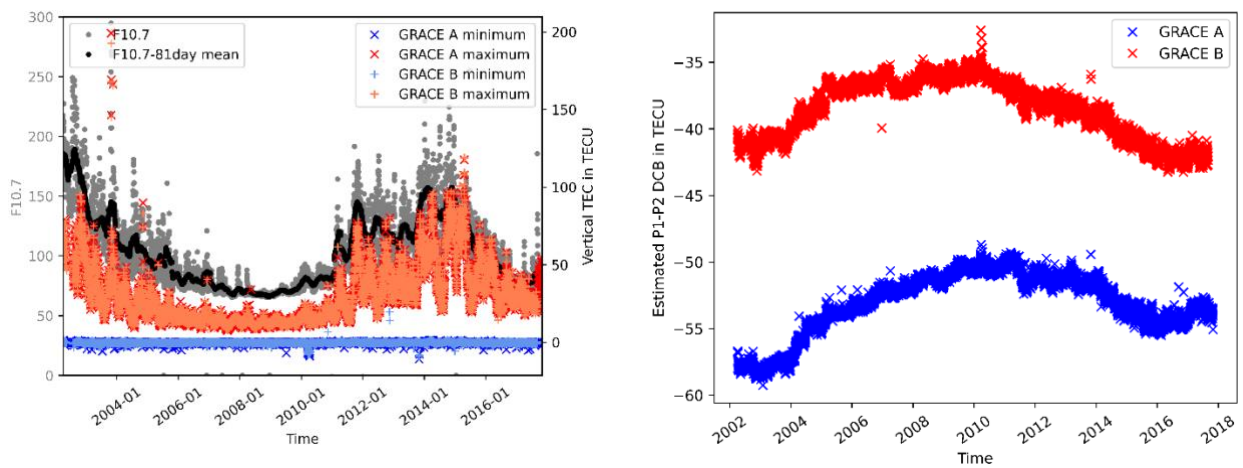


Figure 3.1-6. Same as Figure 3.1-5 but for GRACE.

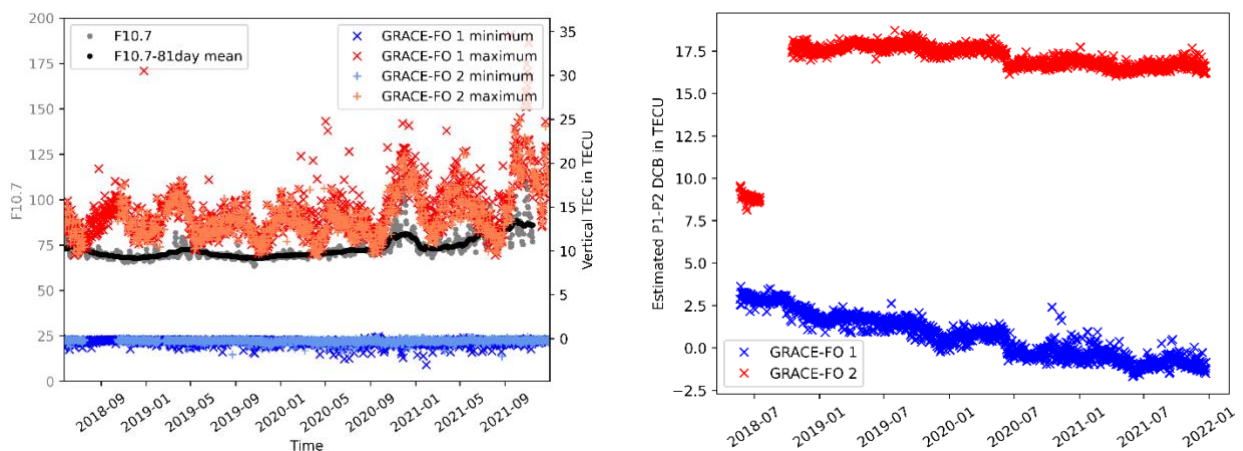


Figure 3.1-7. Same as Figure 3.1-5 but for GRACE-FO.

range of 1-2 TECU with a period of a few months indicate a temperature dependency with local time. For GRACE, four large outliers exist, three for GRACE B and 1 for GRACE A, also caused by too few observations available for DBC estimation. In that case, the receiver bias is set to 0 (not shown in the figure, files are

removed). Like CHAMP, oscillation up to 2 TECU occur in correlation with local time precession. This is to be expected, as the GPS receiver and the satellite design are nearly identical. For GRACE-FO such oscillations in the receiver specific P1-P2 bias are not observed. However, a pronounced jump in the estimated P1-P2 DCB is visible for GRACE-FO. This jump coincides with the on board switch of the instrument processing unit at the beginning of the mission and can thus be assumed to be hardware related [RD-7].

3.1.4 Intersatellite comparisons during conjunctions

The calibrated satellite missions have an overlap with at least one other satellite mission for which TEC is provided in the DISC framework. CHAMP overlaps with GRACE, GRACE overlaps with GOCE and Swarm, Swarm overlaps with GRACE-FO. High consistency of the derived TEC values overall overlaps can thus ensure a homogeneous time series and serve as an error estimate.

The criteria selected for identifying conjunctions is a difference of less than 2° in both, latitude and longitude. The observations must be taken nearly simultaneously within half the sampling interval to ensure a nearly identical timestamp, i.e., 5 s for 10 s sampling (CHAMP, GRACE, GRACE-FO) and 0.5 s for 1 s sampling (GOCE, Swarm). Both satellites must observe the same PRN and the elevation must be higher than 70° to avoid mapping uncertainties.

The expected difference in vertical TEC due to different altitudes of the LEO satellite is compensated using the IRI-2016 model [RD-1] with the default NeQuick [RD-8] topside. The electron density is vertically integrated between the altitude of the lower satellite up to the altitude of the higher satellite. The integration is performed numerically by using Gauss Legendre Quadrature with 6 support points.

The accuracy of the absolute GPS derived TEC is essentially limited by the accuracy of the code levelling and the receiver bias estimation. Assuming a typical (CW)-code noise of 1 m the expected level-ling uncertainty over a typical arc length of 100 observations is close to 2 TECU. Typical uncertainties of the receiver bias are slightly above 1 TECU, which results in total uncertainty of about 3 TECU. To ensure the good quality of the derived TEC products, we, therefore, expect the difference of the conjunctions to be in that range. However, we also must expect uncertainties stemming from the integrated electron density from the IRI model. Those increase with the altitude difference of the satellites.

3.1.4.1 CHAMP and GRACE

CHAMP and GRACE (A/B) have repeating time spans of multiple conjunctions. Those are in northern springs 2003 and 2005, northern winters 2006/2007 and 2008/2009. The altitudinal difference between CHAMP and the GRACE satellites ranged from 80 km in 2003 up to 145 km in 2009. The numbers of conjunctions (for given PRN and elevation restrictions) are 1868 (CHAMP-GRACE A) and 1872 (CHAMP-GRACE B). Numerous conjunctions are observed in all latitudinal and longitudinal regions, and a reasonable sampling is given in magnetic local time and magnetic latitude (see Figure 3.1-8).

Without correction of the TEC difference due to altitude by IRI, an offset of 2 to 2.5 TECU between the simultaneously observed TEC values is observed. The largest standard deviation occurs for the differences between CHAMP and GRACE A with above 3 TECU. After compensating for the different altitudes using the IRI-2016 model (default settings), the mean difference drops nearly to 0 (-0.3 TECU for CHAMP-GRACE A and -0.4 TECU for CHAMP-GRACE B), whereas the standard deviation is well below the targeted 3 TECU with 2.4 TECU and 2.1 TECU, respectively (see Figure 3.1-9). In addition, the distribution of the differences is nearly Gaussian. These results are encouraging and may hint at an even better agreement, since some uncertainty may still be introduced by using the climatological IRI model.

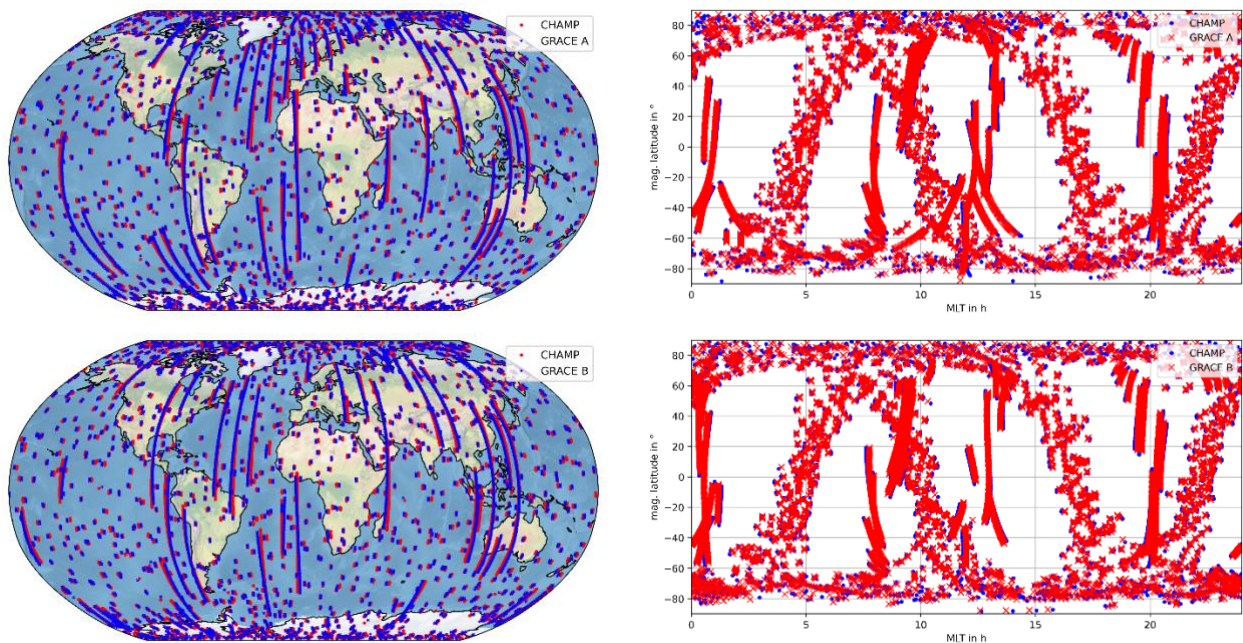


Figure 3.1-8. Distribution of CHAMP and GRACE (A top, B bottom) conjunctions in geographic and geomagnetic coordinates.

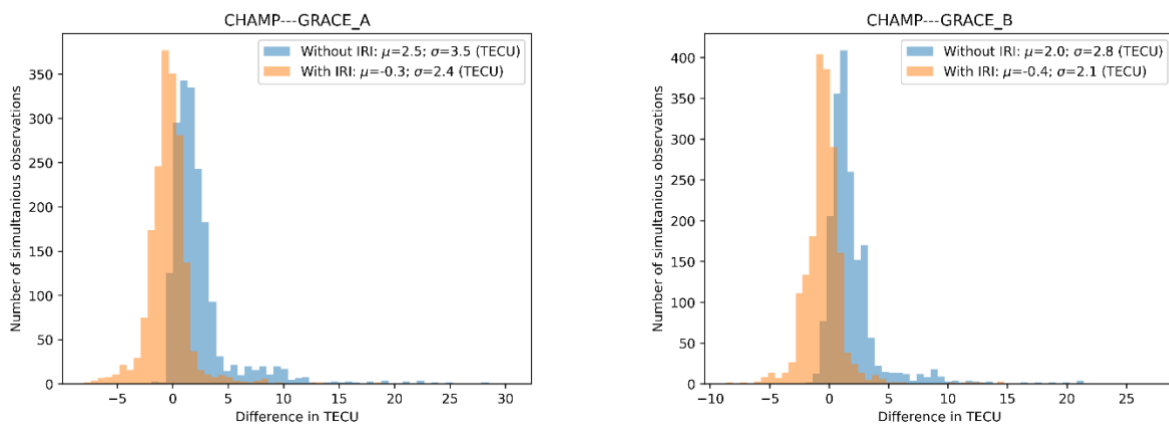


Figure 3.1-9. Histogram of TEC differences at conjunction points for CHAMP and GRACE. Blue: without IRI compensation of TEC and orange: with IRI TEC compensation.

3.1.4.2 GRACE and GOCE

Despite the GOCE's mission duration of only 4 years (from March 2009 until November 2013), there occurred 1460 (GRACE A) and 1488 (GRACE B) conjunctions with GRACE. The geographical coverage of these conjunctions is extensive; however, the local time distribution is limited because of the nearly local time fixed dusk-dawn orbit of GOCE (see Figure 3.1-10).

The altitudinal difference between the spacecraft is roughly 200 km and the conjunctions take place in co- and counter-rotating orbits (conjunctions occur approximately every four months). Without TEC compensation by the IRI model, the offset is large, with 7.5 and 6.4 TECU, whereas the standard deviation is also large with 7.2 and 6.5 TECU for GRACE A and GRACE B, respectively. After TEC compensation by IRI, the mean drops to -0.4 and -0.6 TECU and the standard deviation to 4.2 and 3.8 TECU (see Figure 3.1-11). This is

slightly above the targeted 3 TECU, however, still satisfactory in view of the large altitude difference, and in view of the local time of the difference. Sunrise and sunset times are known to show the least regular behaviour and are consequently difficult to model by IRI.

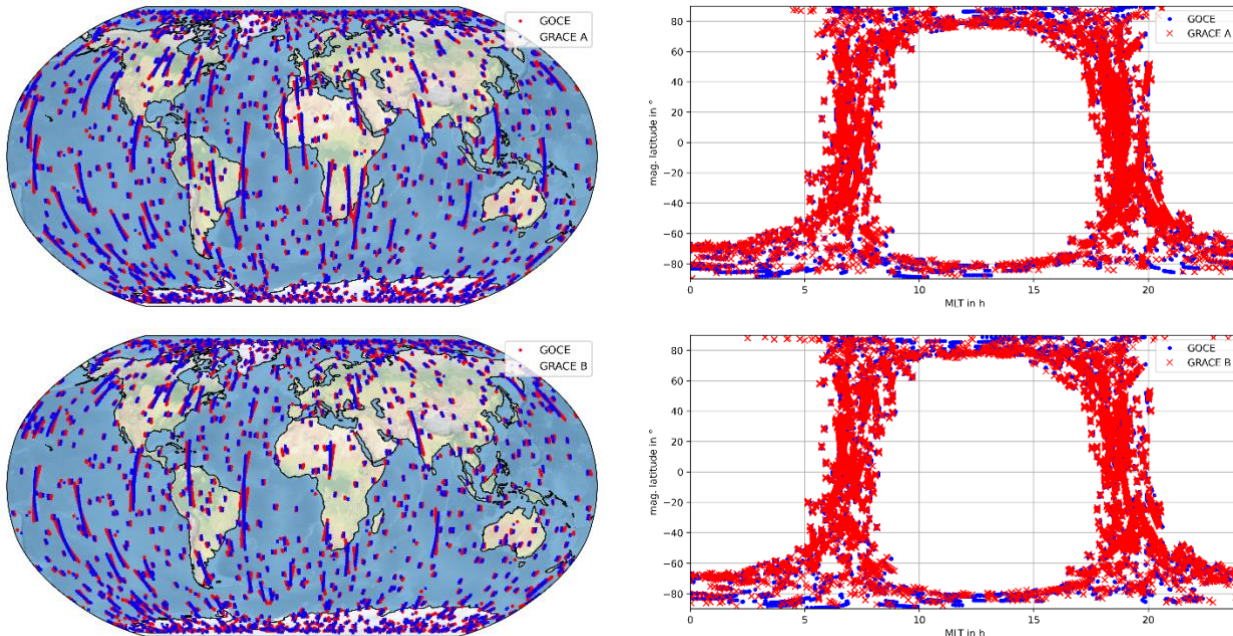


Figure 3.1-10. Distribution of GOCE and GRACE (A top, B bottom) conjunctions in geographical and geomagnetic coordinates.

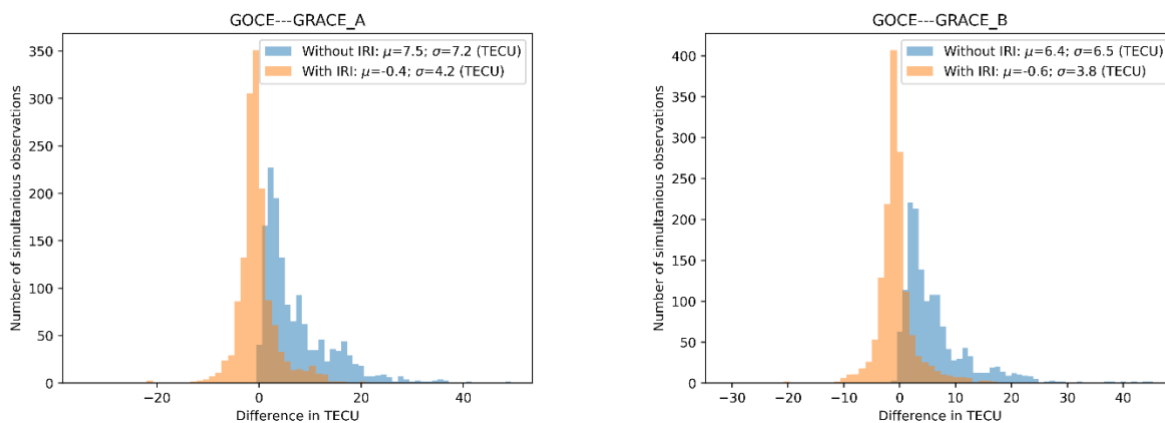


Figure 3.1-11. Histogram of TEC differences at conjunction points for GOCE and GRACE. Blue: without IRI compensation of TEC and orange: with IRI TEC compensation.

3.1.4.3 GRACE and Swarm

Swarm A and GRACE A and GRACE B were in the co-rotating phase in northern spring 2015. For GRACE A there was also a counter-rotating phase in 2017 when data was no longer available from GRACE B (see Figure 3.1-12). The number of conjunctions for GRACE A is thus significantly larger with a total of 733 compared to GRACE B with 460 conjunctions. The altitudinal difference is 65 km in 2015 and 125 km in 2017. The mean and standard deviation without compensation by IRI is already below 2 TECU. With the TEC compensation provided by the IRI model, the differences show a near-zero mean (0.3 TECU and 0.4 TECU) and a standard

deviation of only 1.1 TECU for both satellites (see Figure 3.1-13). This is well below the targeted 3 TECU. As in the comparison between GRACE and GOCE, the conjunctions are near dusk and dawn. Nevertheless, the altitudinal difference is smaller, such that the impact of the model is less pronounced.

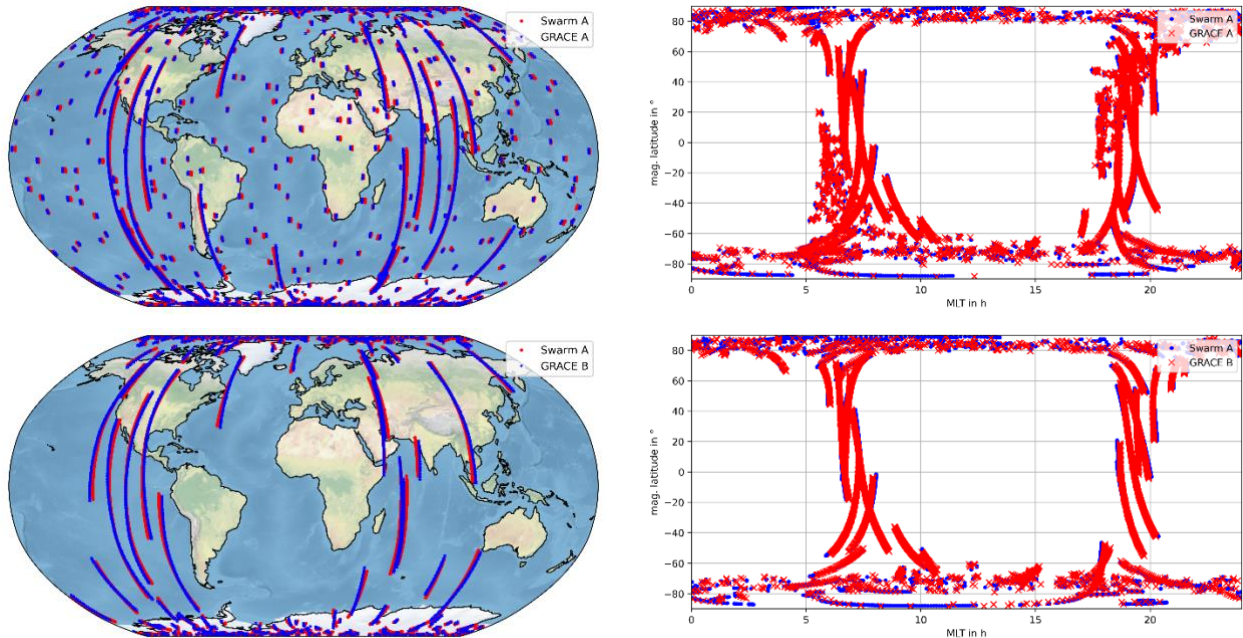


Figure 3.1-12. Distribution of Swarm A and GRACE (A top, B bottom) conjunctions in geographical and geomagnetic coordinates.

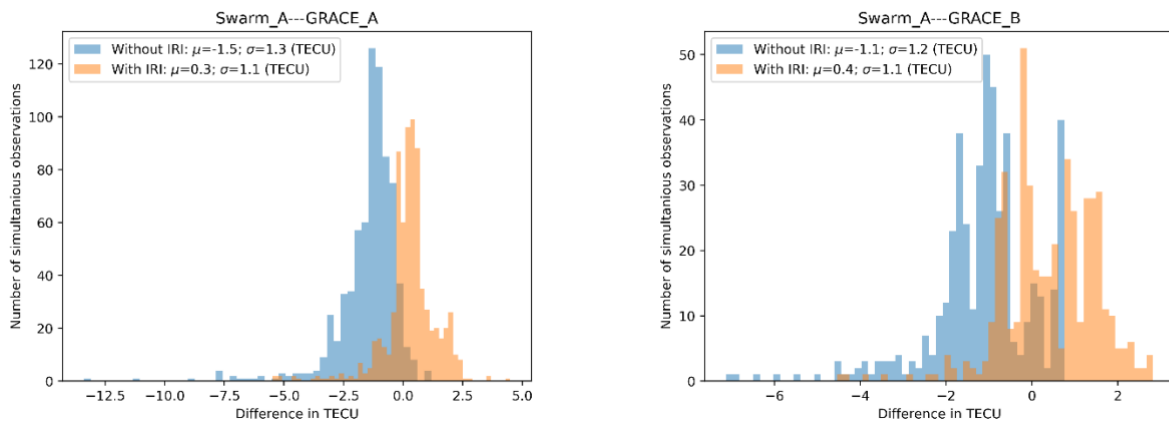


Figure 3.1-13. Histogram of TEC differences at conjunction points for Swarm A and GRACE. Blue: without IRI compensation of TEC and orange: with IRI TEC compensation.

For Swarm B only one co-rotating phase occurred in northern spring 2016 (see Figure 3.1-14) with an altitudinal difference of about 135 km. The number of conjunctions is 601 (GRACE A) and 836 (GRACE B). For GRACE A the differences in the uncompensated and compensated case are both small. For example, in the compensated case, the offset is only 0.1 TECU, and the standard deviation is at 1 TECU (see Figure 3.1-15) for GRACE A. For GRACE B these values are in general larger, and differences of up to 10 TECU can be observed. This might be related to interruptions since GRACE B was entering Earth's shadow in northern spring 2016 and several instruments were switched off.

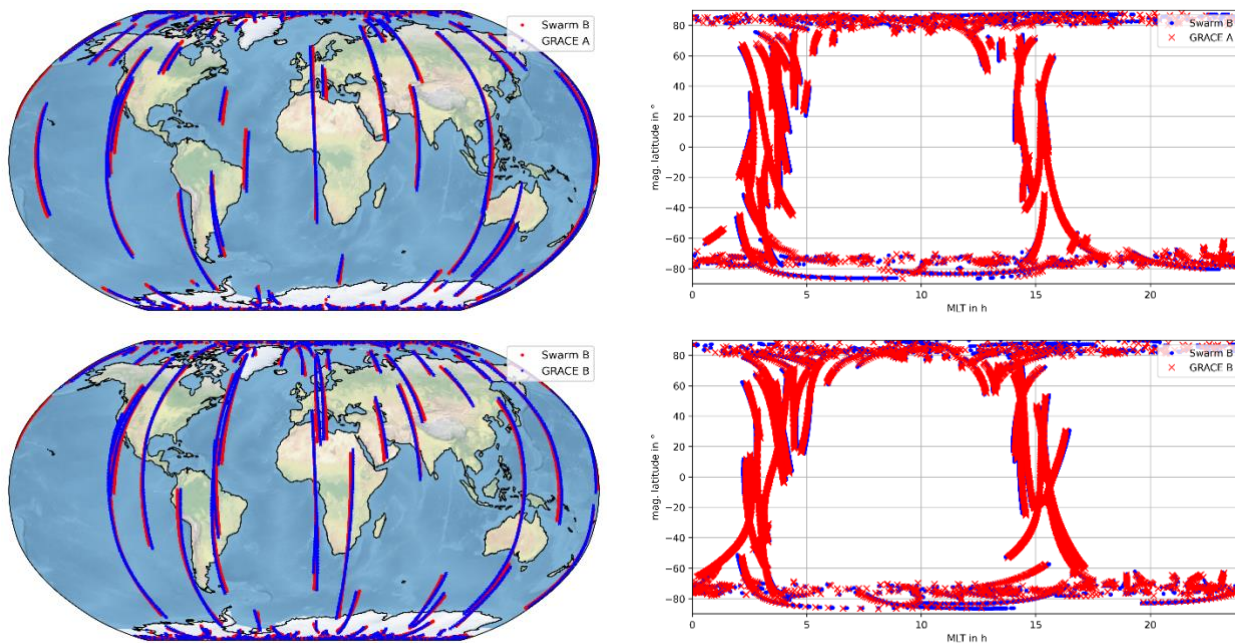


Figure 3.1-14. Distribution of Swarm B and GRACE (A top, B bottom) conjunctions in geographical and geomagnetic coordinates.

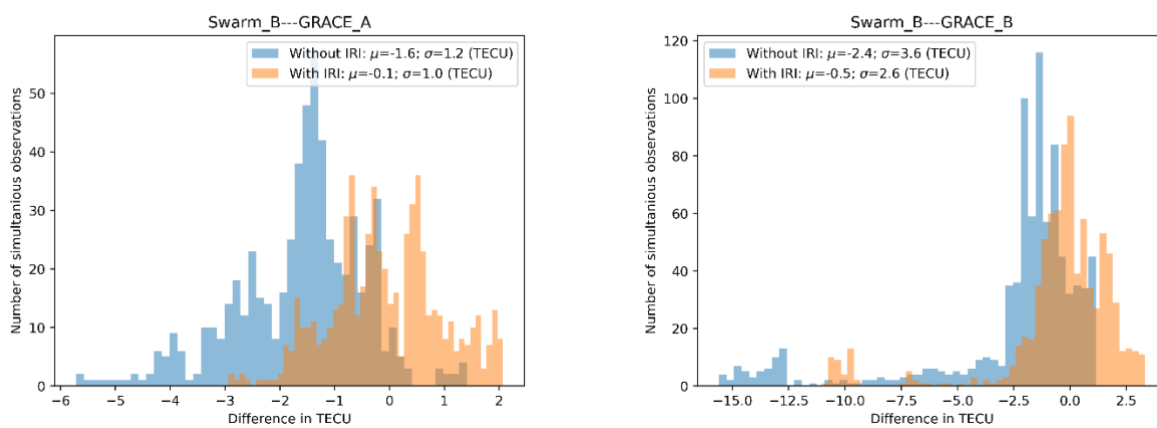


Figure 3.1-15. Histogram of TEC differences at conjunction points for Swarm B and GRACE. Blue: without IRI compensation of TEC and orange: with IRI TEC compensation.

For Swarm C, pretty much the same conditions hold as for Swarm A, as the satellites are co-located. There is again a co-rotating phase in 2015 and the counter-rotating phase in 2017 was only seen for GRACE B (see Figure 3.1-16). The numbers of conjunction are 692 and 635. The increase in quality compared to Swarm A is likely caused by the tracking loop updates performed on Swarm C. For GRACE A, again a similar performance is achieved with an offset of only 0.1 TECU and a standard deviation of 1.2 TECU after compensation. For GRACE B the compensation causes a small increase in the mean, from -0.6 TECU to 0.9 TECU, whereas the standard deviation decreases from 1.7 TECU to 1.4 TECU (see Figure 3.1-17). Nonetheless, a mean of below 1 TECU hints at a high-quality comparison.

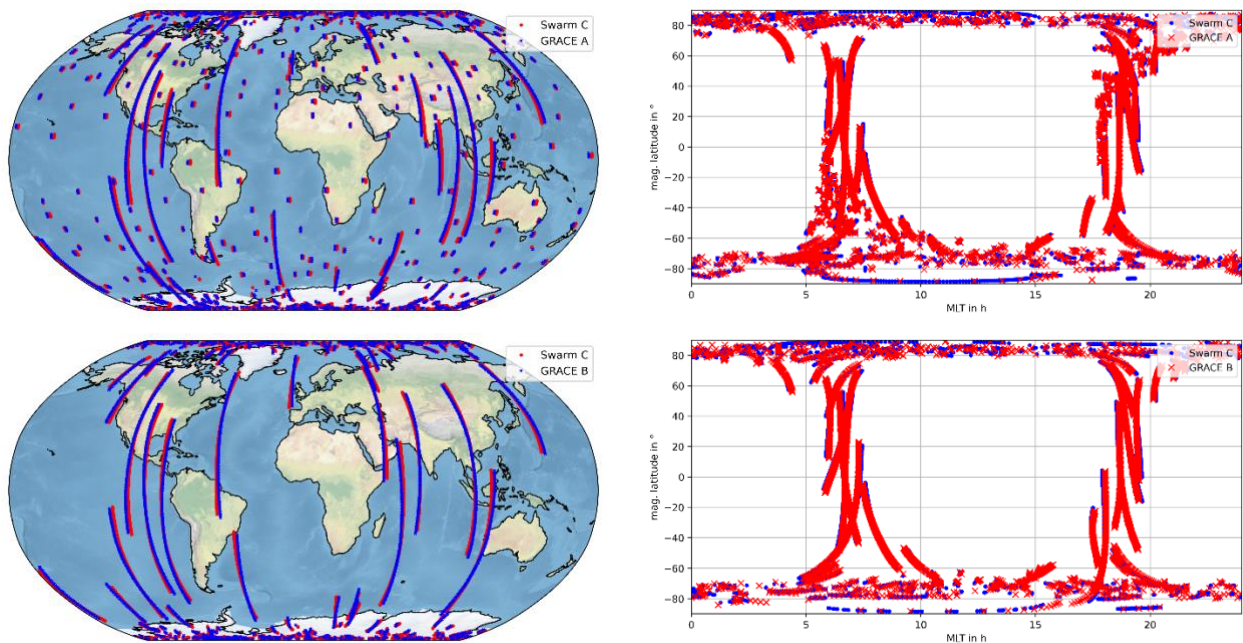


Figure 3.1-16. Distribution of Swarm C and GRACE (A top, B bottom) conjunctions in geographical and geomagnetic coordinates.

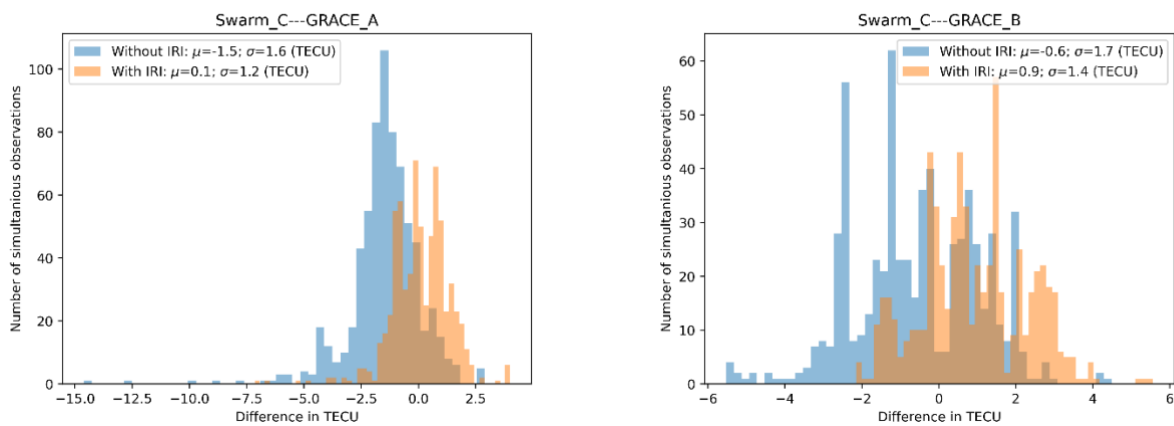


Figure 3.1-17. Histogram of TEC differences at conjunction points for Swarm C and GRACE. Blue: without IRI compensation of TEC and orange: with IRI TEC compensation.

Overall, the conclusion can be drawn, that the GRACE and Swarm TEC time series are highly consistent.

3.1.4.4 Swarm and GRACE-FO

Swarm A (and Swarm C) have a co-rotating phase with GRACE-FO in May/June 2020 (see Figure 3.1-18). For Swarm A the number of conjunctions is 504 (GRACE-FO 1) and 508 (GRACE-FO 2). Due to the very low solar activity and the altitude difference of only approximately 60 km, the impact of the IRI model is negligible. Offsets below 1 TECU are observed and a standard deviation of 1.2 TECU and 0.9 TECU (see Figure 3.1-19) matching the performance of the comparison of Swarm and GRACE (see Figure 3.1-13, Figure 3.1-15, Figure 3.1-17).

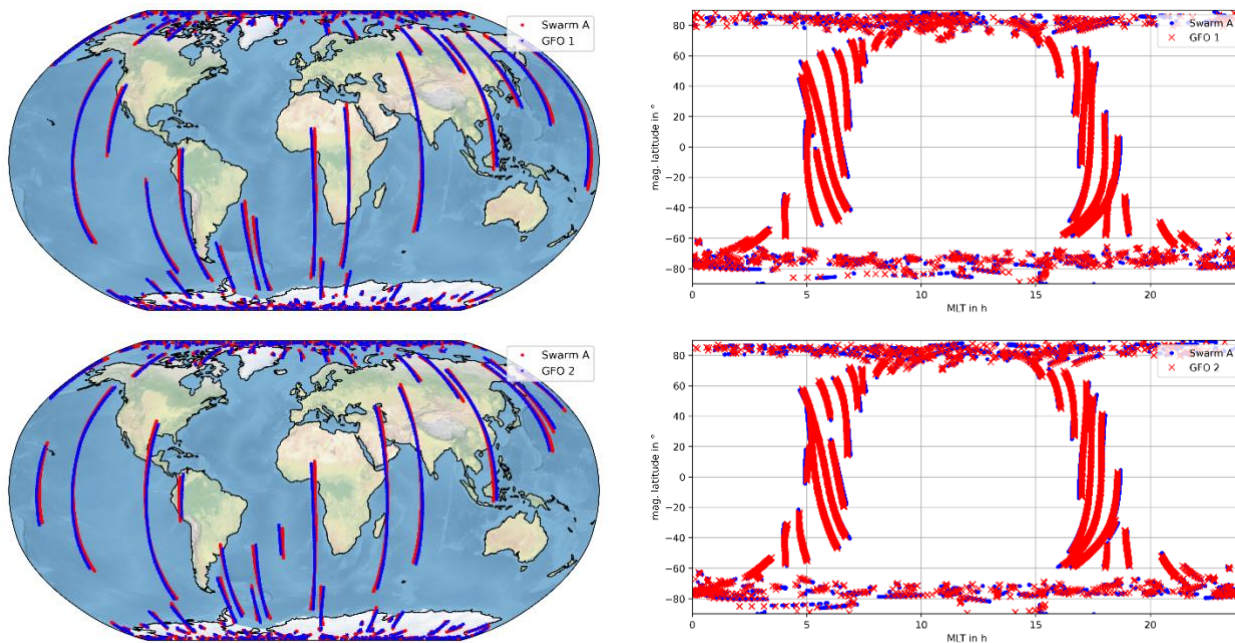


Figure 3.1-18. Distribution of Swarm A and GRACE-FO (1 top, 2 bottom) conjunctions in geographical and geomagnetic coordinates.

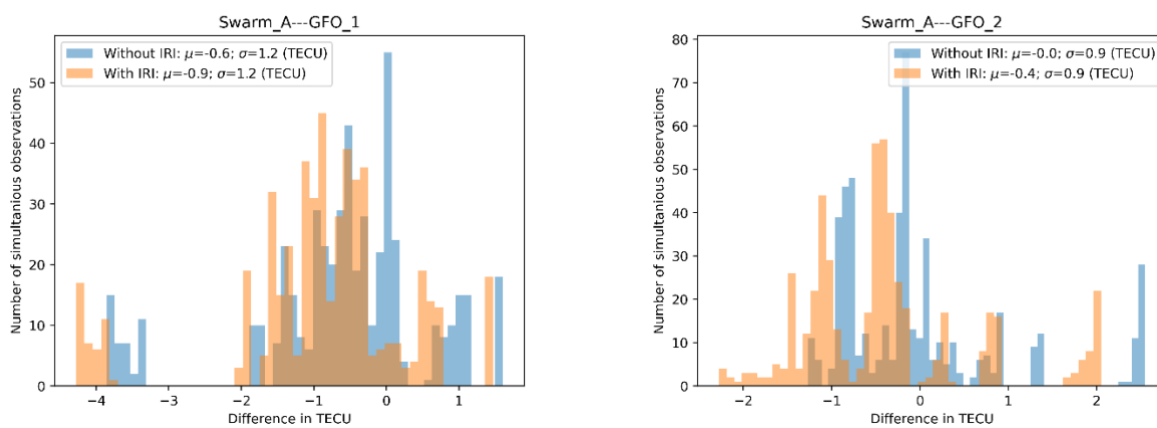


Figure 3.1-19. Histogram of TEC differences at conjunction points for Swarm A and GRACE-FO. Blue: without IRI compensation of TEC and orange: with IRI TEC compensation.

Especially the comparison of Swarm B with GRACE-FO is of interest, as from October until December 2019 Swarm B and GRACE-FO were in counter-rotating orbits. This resulted in numerous conjunctions with nearly global coverage. The satellites are at a very similar altitude with differences below 20 km. The global coverage of the conjunctions is extremely good, whereas they are highly localized in the geo-magnetic local time and latitude (see Figure 3.1-20). The very low difference in altitude does not necessarily require an altitudinal TEC compensation by IRI. In total 787 (GRACE-FO 1) and 762 (GRACE-FO 1) conjunctions were found until the end of 2021. The offset is in all cases below 0.4 TECU and the standard deviation does not exceed 1 TECU (see Figure 3.1-21). The conclusion may be drawn, that the TEC obtained by Swarm B and by GRACE-FO are consistent on a superior level exceeding the expectations.

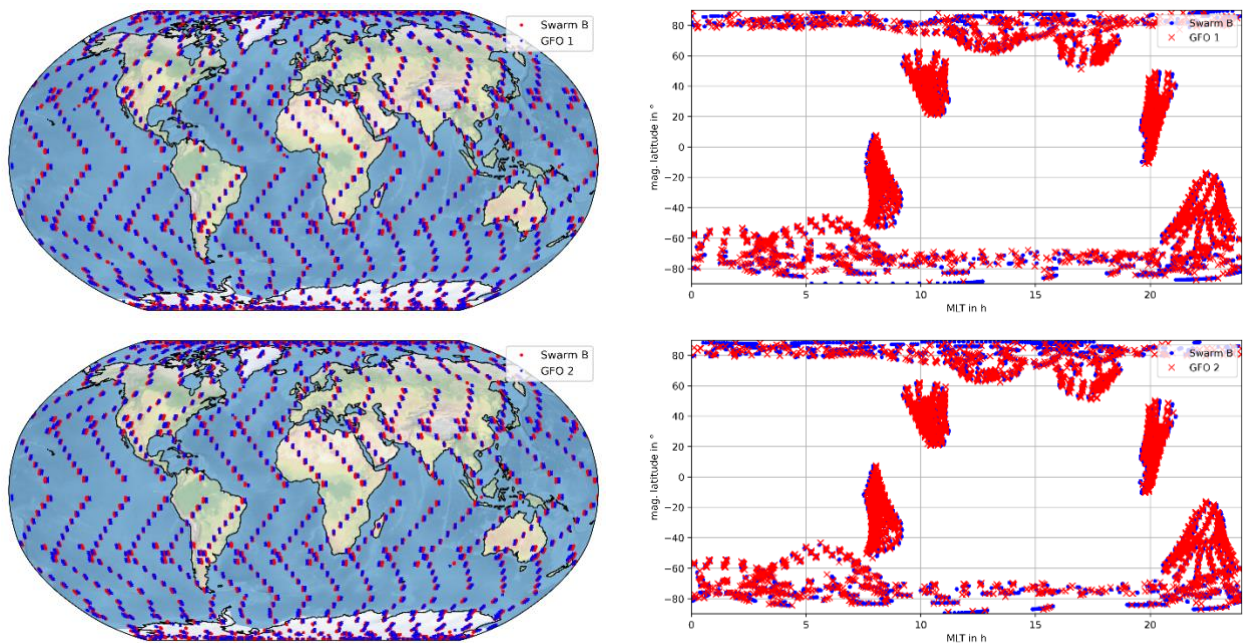


Figure 3.1-20. Distribution of Swarm B and GRACE-FO (1 top, 2 bottom) conjunctions in geographical and geomagnetic coordinates.

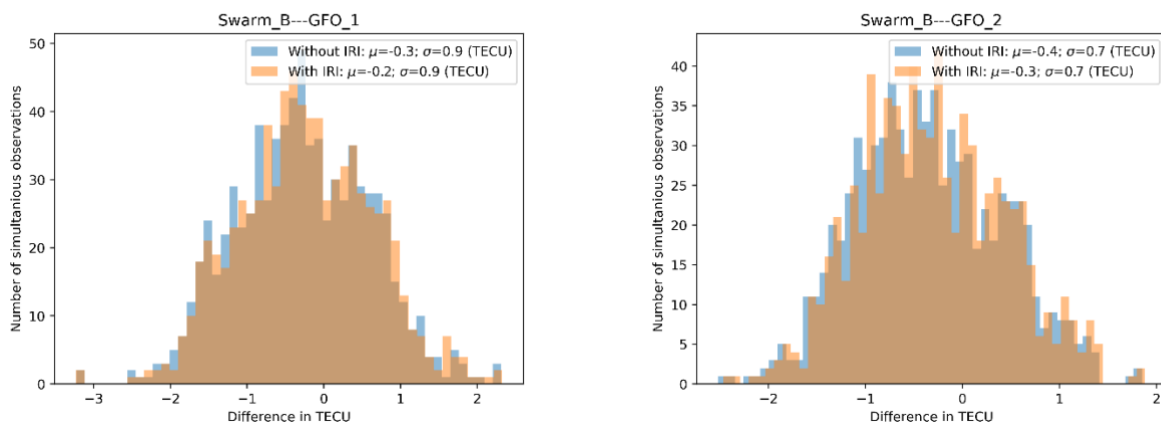


Figure 3.1-21. Histogram of TEC differences at conjunction points for Swarm B and GRACE-FO. Blue: without IRI compensation of TEC and orange: with IRI TEC compensation.

Swarm C again matches the conclusions already obtained from Swarm A. Offset and standard deviation are on a similar level. Swarm C provides additional 507 and 467 conjunctions from the co-rotating phase in May/June 2020 (see Figure 3.1-22 and Figure 3.1-23).

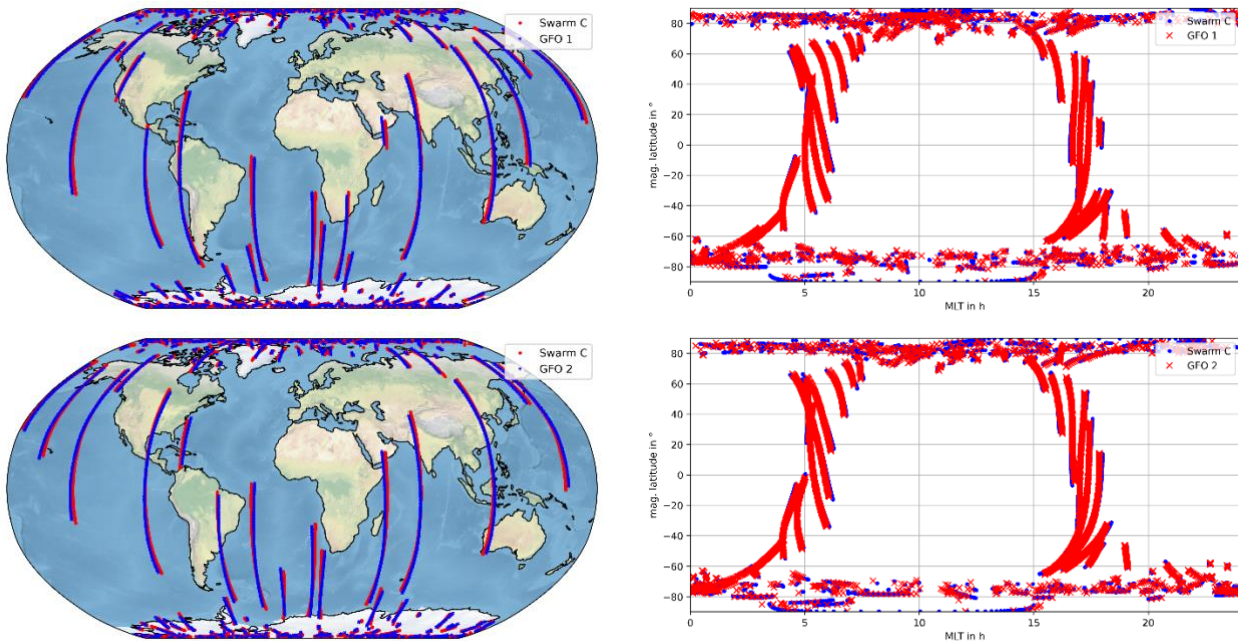


Figure 3.1-22. Distribution of Swarm C and GRACE-FO (1 top, 2 bottom) conjunctions in geographical and geomagnetic coordinates.

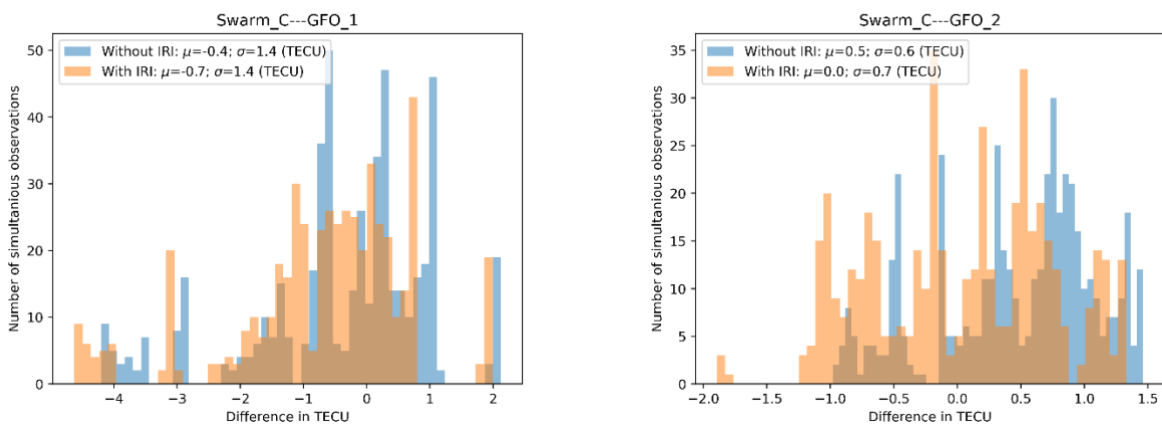


Figure 3.1-23. Histogram of TEC differences at conjunction points for Swarm C and GRACE-FO. Blue: without IRI compensation of TEC and orange: with IRI TEC compensation.

3.2 K-Band ranging (KBR) electron density

The ionization in the topside ionosphere is mainly driven by solar electromagnetic radiation. The proxy of solar radiation is the solar flux index F10.7. At a fixed altitude, latitude and local time, the electron density is expected to be well correlated to the F10.7 index. Figure 3.2-1 displays the evolution of daily means of KBR derived electron densities from the GRACE and GRACE-FO missions and of the F10.7 index. Especially for GRACE, the electron density is strongly correlated with the F10.7 index. The electron density during the solar maximum 2013-2015 is higher than during the solar maximum 2003 due to the lower altitude of the GRACE satellites at the end of their mission. Strong monthly patterns in GRACE electron densities are caused by the local time precession of GRACE. For GRACE-FO the mean electron density observed during solar minimum conditions in 2020 is significantly below the electron density observed by GRACE near the solar minimum

conditions near 2008. This again is caused by the altitudinal differences. GRACE-FO in 2020 is near 502 km altitude, whereas GRACE was at an average altitude of 472 km.

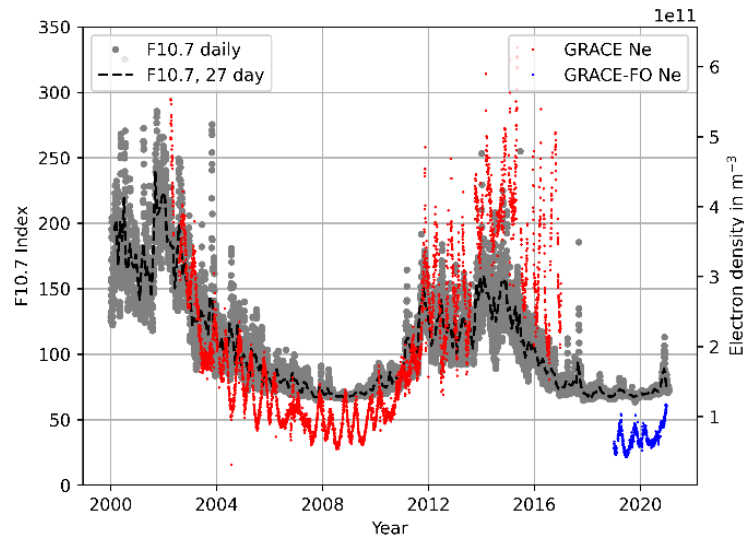


Figure 3.2-1. Mean electron density observed by GRACE (red) and GRACE-FO KBR (blue) compared to the F10.7 solar flux index.

3.2.1 Validation with radar observations

Radar observations of the topside ionosphere provide independent means for validation. Incoherent Scatter Radars (ISRs) provide nearly vertical profiles of electron density between about 200 to 500 km altitude above their location. These data are publicly available via the [MADRIGAL database](#)¹. The following validation study applies observations from the ISRs located at Millstone Hill, Arecibo, Resolute Bay, Jicamarca, Poker Flat, and from EISCAT. The location of the ISR stations is provided in Figure 3.2-2.

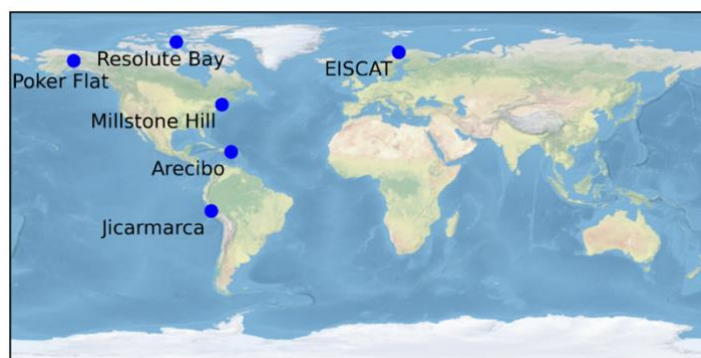


Figure 3.2-2. Radar stations used for validation of the KBR derived electron density.

Since the radar profiles provided by the observation files obtained from the MADRIGAL database are typically samples with several kilometres spacing, an interpolation is performed to estimate the electron density directly at the satellite altitude. The interpolation itself is performed on $\log_{10}(Ne(h))$, where h is the altitude of the specific sample points. A quadratic polynomial is fitted using least-squares from 100 km below satellite altitude to 100 km above satellite altitude. To ensure a good interpolation, a minimum of one

¹ <http://millstonehill.haystack.mit.edu/index.html>.

measurement of the radar must be within 20 km of the satellite altitude, and the distribution of radar observations is not allowed to be one-sided, i.e., not all observations are exclusively above or exclusively below the satellite altitude. As a basis, all available data meeting the conjunction criteria (see below) are stored. If additional error estimates to the radar observations were provided via the MADRIGAL database, they were utilized to weight the least-squares fit accordingly. The data is screened within a 3-sigma radius of the polynomial fit and the fit is repeated on the screened data to further refine the fit. The conjunction criteria are:

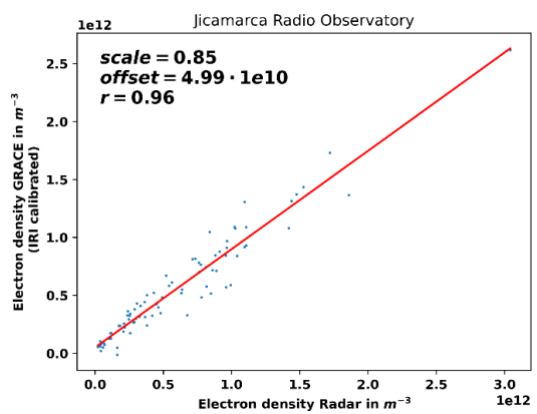
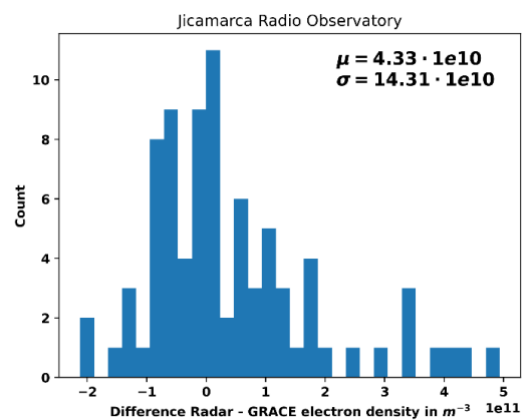
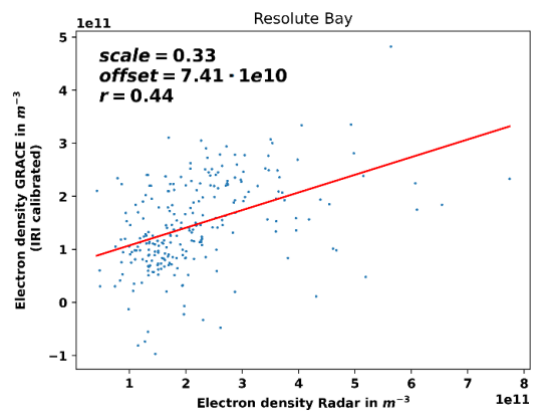
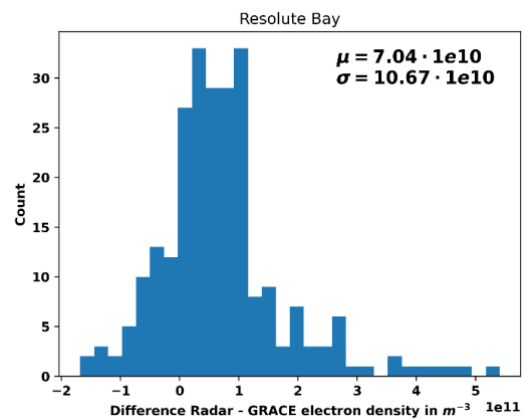
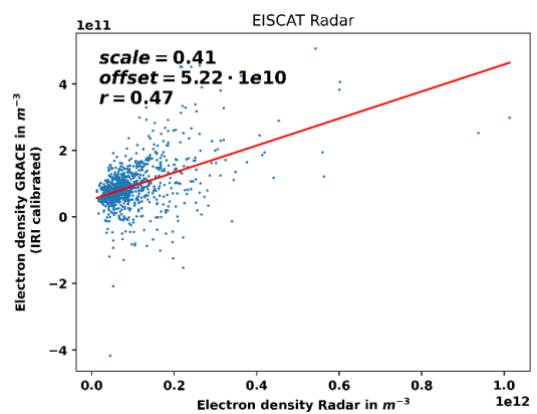
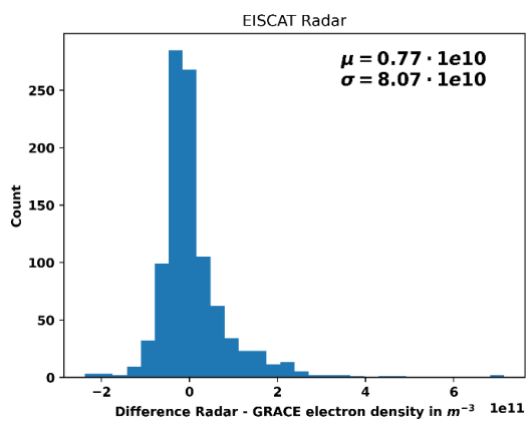
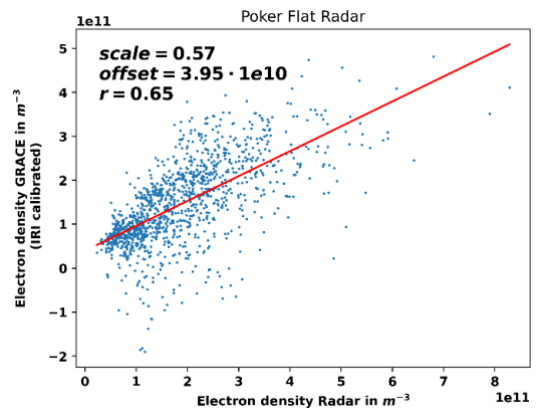
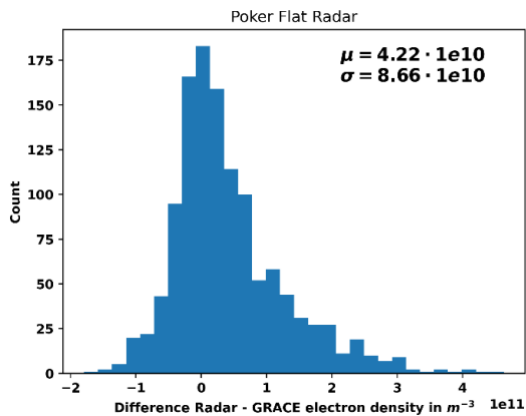
- Satellite within 5° longitude of the radar station;
- Satellite within 5° latitude of the radar station;
- Maximum 15 minutes between radar measurement and overflight;
- At least one observation within ± 20 km of satellite altitude;
- Radar observations exist below and above satellite altitude.

The number of conjunctions is provided in Table 3.2-1. For each conjunction, the difference (offset) between the conjunctions is independently and combined considered and the offsets to the IRI calibrated electron density values from the GRACE and GRACE-FO missions are compared to the values of the radar observations at the satellite altitude. The results are shown in Figure 3.2-3, Figure 3.2-4 and Figure 3.2-5. For the GRACE KBR measurements, a mean offset to radar data of less than $7.4 \cdot 10^{10} m^{-3}$ can be seen for all individual radars (see Figure 3.2-3). The best correlation is achieved for the equatorial and mid latitude stations (Jicamarca: 0.96, Arecibo: 0.96, Millstone Hill: 0.88), where the electron density profiles are regular and a significant ionization can be observed at GRACE altitude. Regarding the number of conjunctions (Table 3.2-1), EISCAT is contributing by far the most conjunctions. However, EISCAT, Poker Flat, and Resolute Bay suffer also from the largest scatter in GRACE altitude regions, which causes large uncertainties and therefore the low scale factor with in the linear fit. The reasons are irregular profiles of electron density in polar regions, in general a low background electron density at GRACE altitude near the poles. The errors provided by the radar stations also increase significantly. If all the radars are combined, only a small mean offset of $1.95 \cdot 10^{10} m^{-3}$ remains, with a standard deviation of $8.32 \cdot 10^{10} m^{-3}$. Large outliers, as they were occasionally observed in single radar observations, are mitigated in the statistics with all radar stations combined. Here, the mean overall radar conjunctions from different stations and timestamps concerning one connected arc in GRACE-KBR measurements are taken to obtain an arc-wise error estimate. In several cases, multiple radar profiles could be combined for arc wise comparison. Therefore, the number of Arcs with conjunctions is significantly smaller than the sum of Radar conjunctions (Table 3.2-1).

Table 3.2-1. Radar conjunctions for GRACE and GRACE-FO (until the end of 2021).

Satellite	# Arcs	Millstone Hill	Arecibo	Resolute Bay	Jicamarca	EISCAT	Poker Flat	# Arcs with conjunction
GRACE	8313	390	131	247	82	988	1215	1138 (13.7%)
GRACE-FO	358	19	0	0	2	13	2	21 (6%) ²

² Actually, there are several more conjunctions. However, the topside profile was not reconstructable due to observational noise of the radar at GRACE(-FO) altitude.



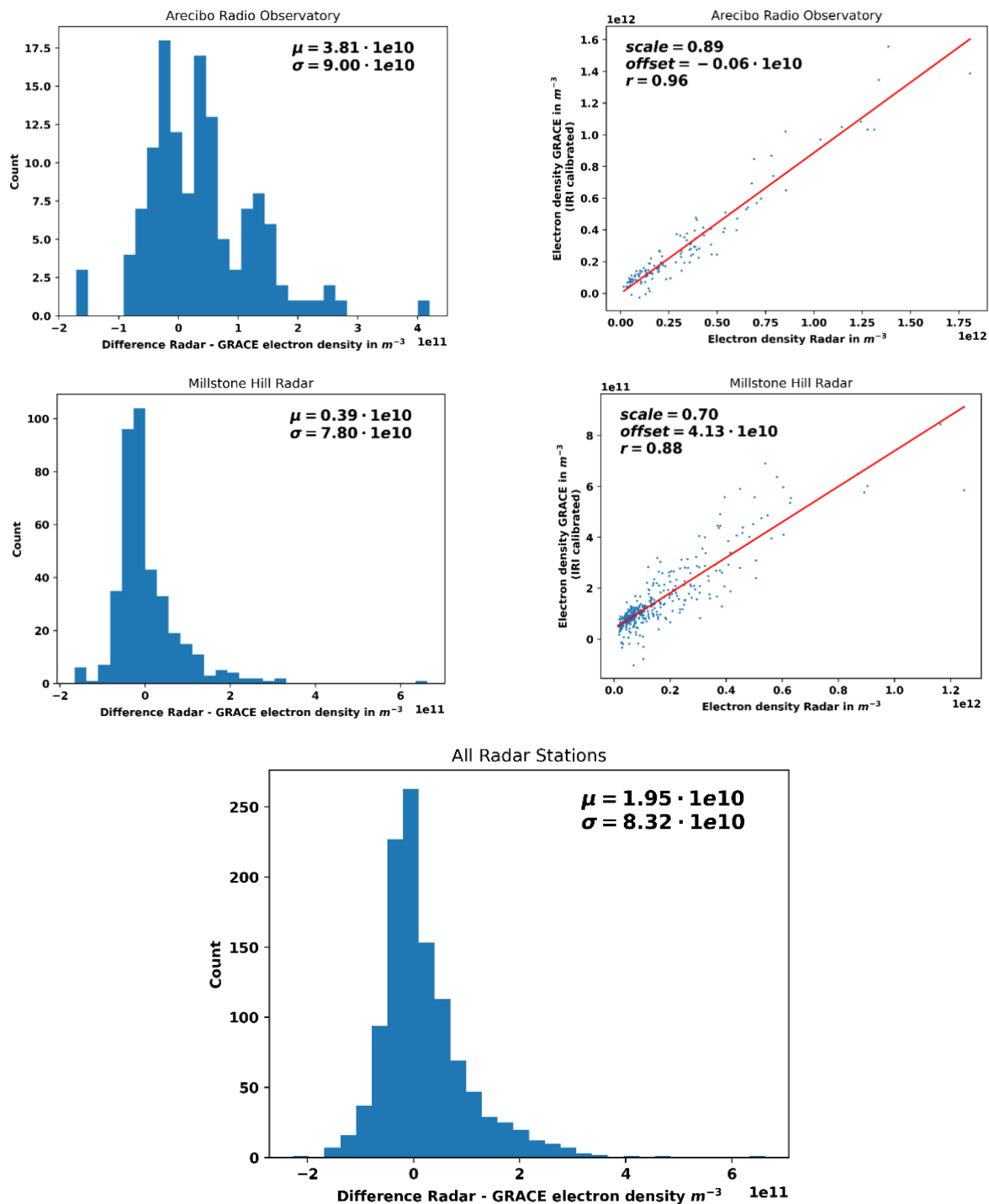


Figure 3.2-3. Calibration differences to radar stations for GRACE. And the correlation between Radar values and the IRI calibrated electron density.

Similar observations are made for GRACE-FO (Figure 3.2-4). Correlation plots were neglected due to the very low number of conjunctions. Again, most of the conjunctions are available for EISCAT followed by Millstone Hill. The comparisons give a mean offset of $-1.91 \cdot 10^{10} m^{-3}$ and a standard deviation of $7.15 \cdot 10^{10} m^{-3}$. The standard deviation is lower compared to GRACE, since because of the larger altitude, the lower background electron density and because IRI predictions, which were used for calibration, correspond better from low to moderate geomagnetic activity periods but cannot reproduce short term variations caused by a geomagnetic storm or rapid variations in solar flux.

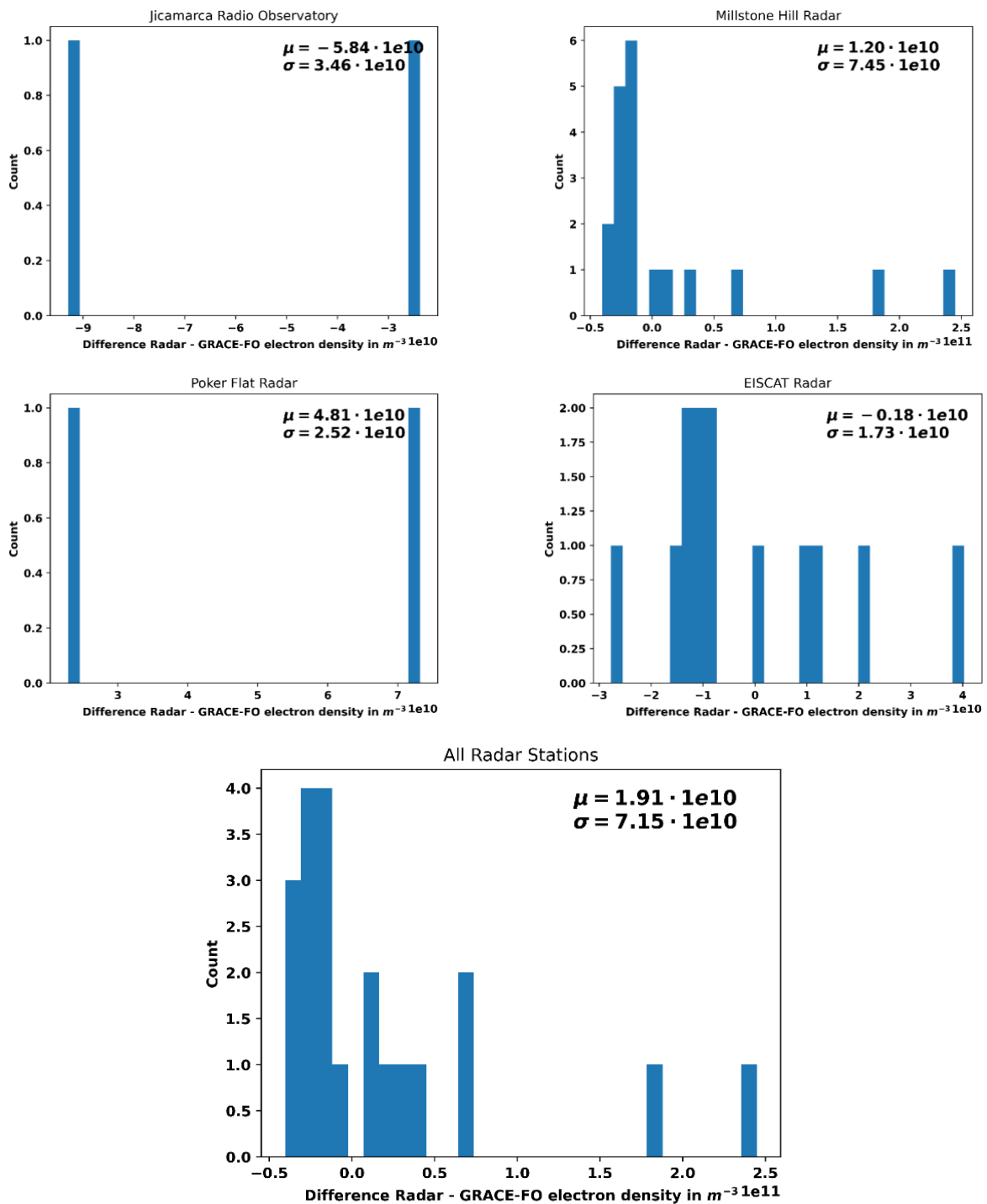


Figure 3.2-4. Calibration differences to radar stations for GRACE-FO.

Figure 3.2-5 presents calibration bias between radar observation and the IRI model together with the F10.7 index. For the GRACE mission, the offsets are largest during solar flux active periods and small during solar minimum. For GRACE-FO, mostly solar minimum conditions are observed and therefore the scatter of the offsets is much smaller compared to GRACE.

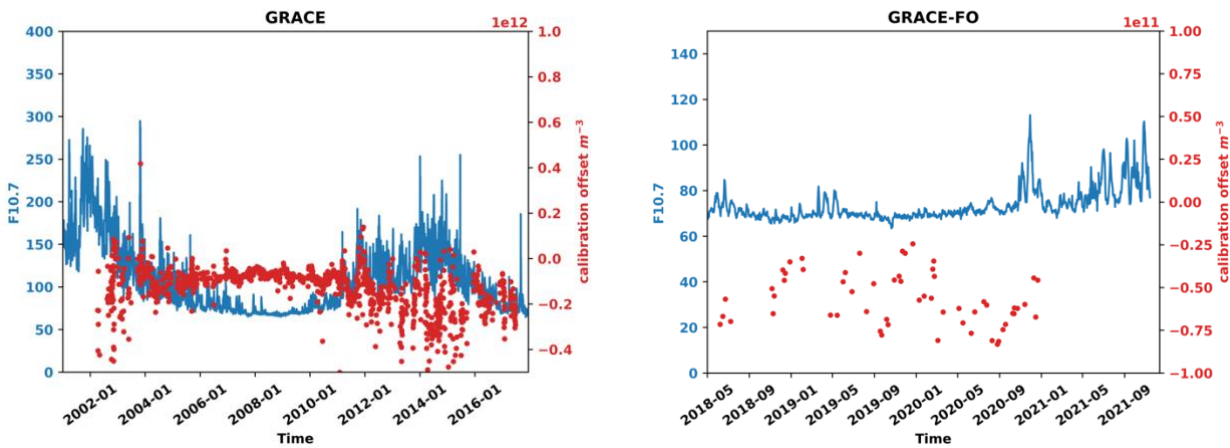


Figure 3.2-5. Radar calibration offsets compared to the F10.7 Index.

3.2.2 Swarm B and GRACE-FO conjunctions

Conjunctions of Swarm B and GRACE-FO are used for electron density validation. Swarm B is equipped with Langmuir probes, capable of measuring in situ electron density. A comparison is carried out for the conjunction data points themselves. We use the most up to date corrected Swarm B electron density data set, e.g., baseline 0601 [RD-9]. The mean offset between Swarm B and GRACE-FO is $0.8 \cdot 10^{10} m^{-3}$, whereas the standard deviation is $6.4 \cdot 10^{10} m^{-3}$. The majority of the Langmuir probe measurements is smaller, however, large positive values exist, which cause the positive mean (see Figure 3.2-6). These values are similar to results of an intercalibration effort of GRACE KBR in [RD-10] where an earlier GRACE KBR electron density dataset was used [RD-11]. Here the offset compared to COSMIC was $-1.8 \cdot 10^{10} m^{-3}$ (GRACE KBR minus COSMIC Ne) with a standard deviation of $6.3 \cdot 10^{10} m^{-3}$. Figure 3.2-6 shows that the vast majority of the offsets is close to zero. Larger offsets of a few $10^{11} m^{-3}$ are observed at low latitudes and when Swarm is a few kilometres below GRACE-FO. In mid or high magnetic latitudes, the differences are much lower. There, the background electron density is lower than at low latitudes resulting in less significant differences.

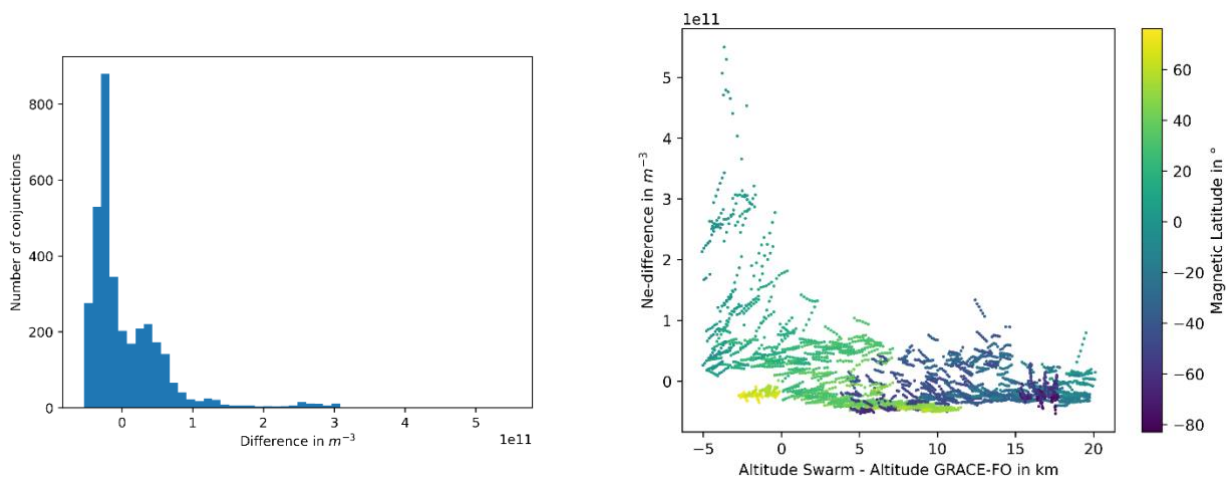


Figure 3.2-6. Histogram of electron density differences at conjunctions between Swarm B and GRACE-FO (left), and scatter plot to compare the differences in electron density to the altitude difference. Colour coding is used to indicate the dependency on magnetic latitude.

3.2.3 Climatology

Ionospheric electron density in magnetic latitude and magnetic local time is assigned to a well-defined global pattern. The electron density peak is observed a few degrees north and south of the geomagnetic equator around 15 LT, which is known as the Appleton Anomaly, and where the largest variability is observed (see upper right panel of Figure 3.2-7). After sunset, the electron density quickly drops, however, the "tails" near $\pm 5^\circ$ to 10° magnetic latitude after sunset may extend a few hours into later local times, sometimes until midnight. The highest ionization is observed in equatorial latitudes, whereas the highest variability takes place in the ionization peaks and the equatorial region after sunset.

Figure 3.2-7 displays the annual mean and the annual standard deviation. Binning is performed in 2° magnetic latitude and 30 minutes in local time. The standard deviation is an essential tool to investigate the homogeneity of the time series since large outliers cause isolated spots of large variations. For GRACE in 2003, the largest variations occur in the equatorial ionosphere between 10 LT and 22 LT. The largest isolated variations near 16:00 LT are caused by the Halloween Storm in 2003 and are not related to data artefacts.

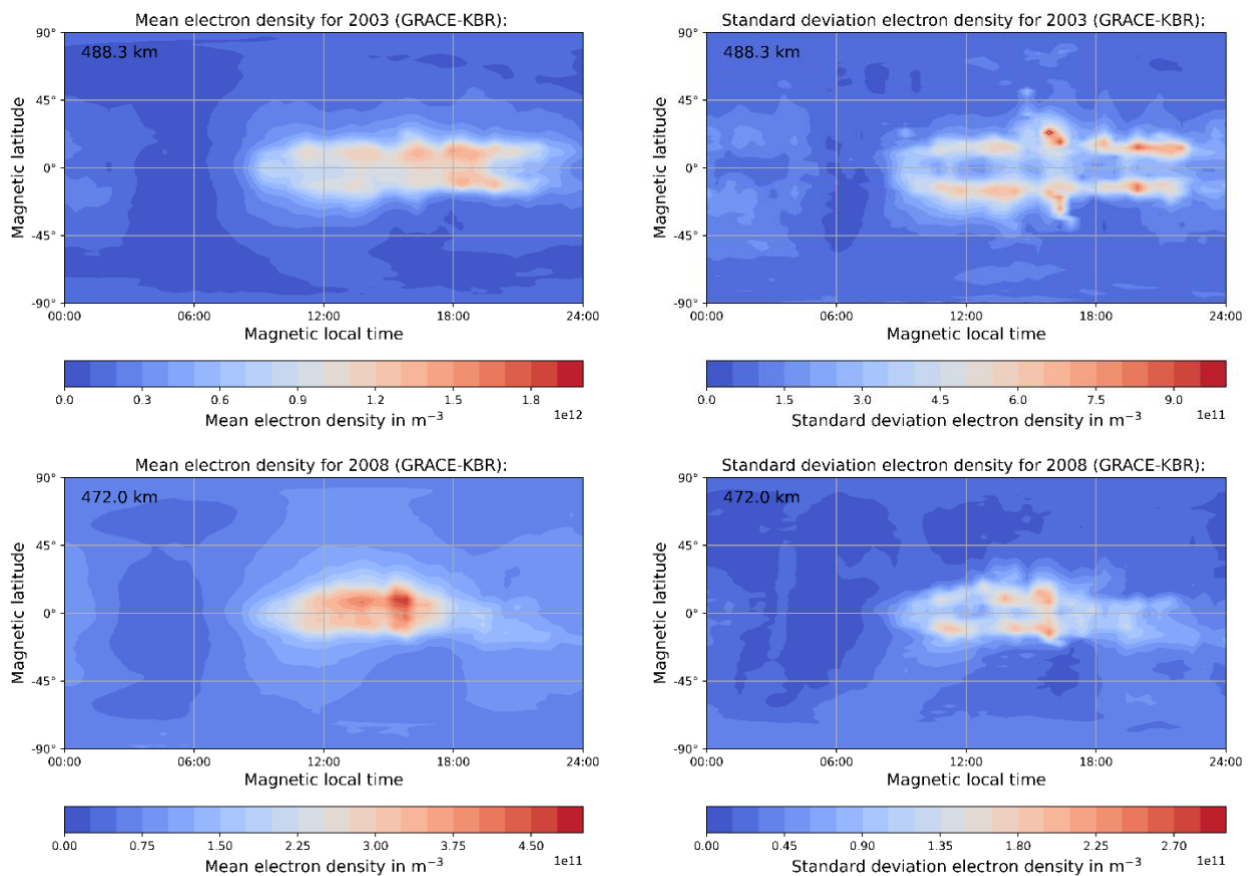


Figure 3.2-7. Mean and standard deviation of GRACE electron density binned in magnetic latitude (2°) and magnetic local time (30 minutes). The solar maximum year 2003 and the solar minimum year 2008 are displayed.

In 2008, during solar minimum conditions, the peak of electron density is localized around the day-side magnetic equator and variation is far less pronounced. The standard deviation is largest near the ionization peaks. Please note the different scale compared to the 2003 scenario. The peak is lower by a factor of 4, whereas the standard deviation in 2003 is less than a third of the standard deviation observed in 2008.

The years 2019 and 2020 are analysed for GRACE-FO (see Figure 3.2-8). 2018 is not included, since GRACE-FO was launched in May 2018 and the KBR instrument had a long downtime in Fall 2018. In 2019 and 2020 the

KBR was nearly continuously operated, and thus electron density may be derived. The years selected are comparable to the 2008 year of GRACE, where the solar flux index was on a similar level. Nevertheless, GRACE-FO observes less ionization, which is caused by the higher altitude of approximately 30 km compared to GRACE in 2008.

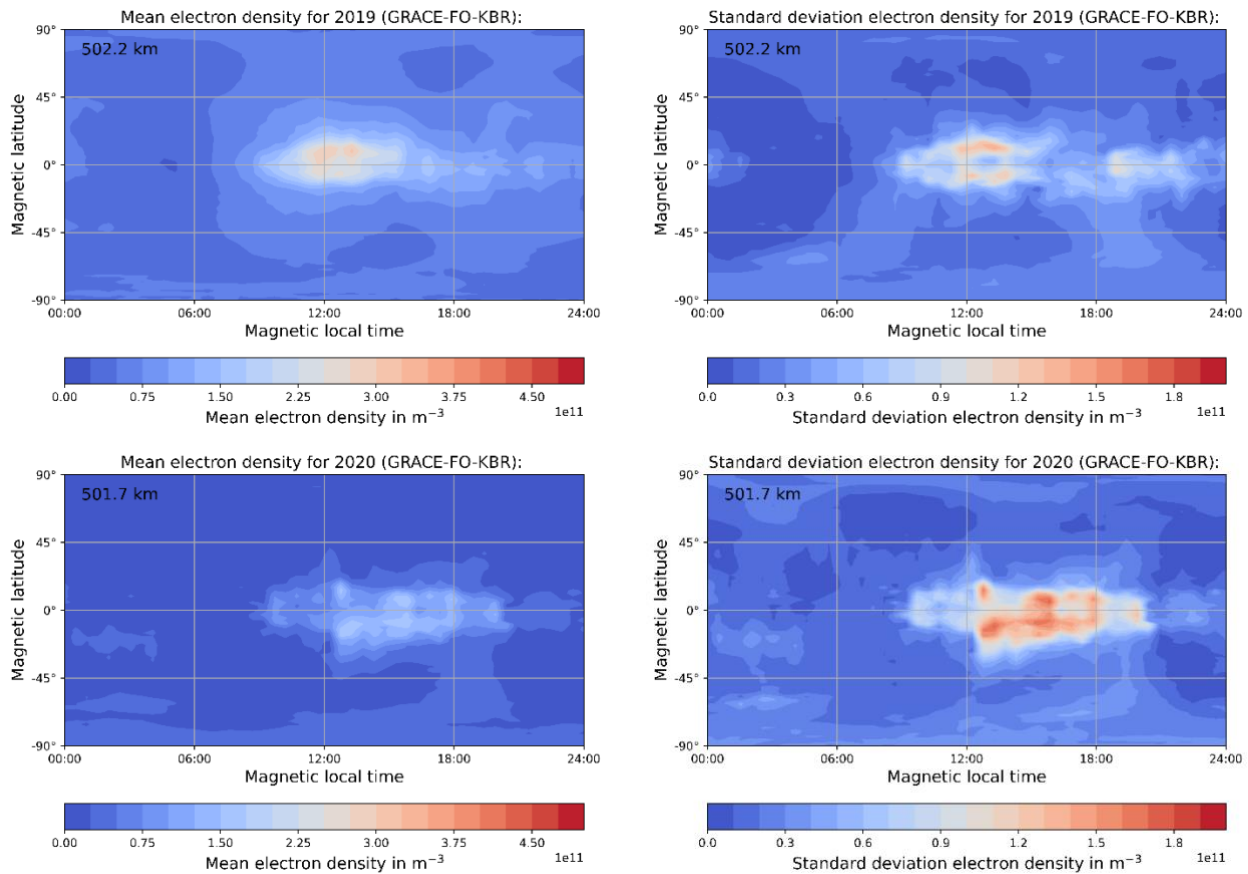


Figure 3.2-8. Mean and standard deviation of GRACE-FO electron density binned in magnetic latitude (2°) and magnetic local time (30 minutes). The years 2019 and 2020 are displayed.

4 Summary and conclusions

This document validates the derived TEC from GPS observables at CHAMP, GRACE, and GRACE-FO and in situ electron density derived from K- and Ka-band observations between the twin satellites of GRACE and GRACE-FO using the processing algorithms outlined in [AD-3] and [AD-5]. Both, internal (single satellite and conjunctions) and external comparisons (IRI-2016 and radar) are used to investigate the quality of the derived products. It is found that the expected accuracy of TEC with below 3 TECU is met and the final product can be expected to be as accurate as 1–2 TECU depending on the mission and solar activity. For all missions considered, it is also found that the amount of data is sufficiently large keeping 70–90% of the observations for most days. This performance is mostly affected by external influences, such as occultation antenna receiver updates, and flex power.

For the electron density, the dependency on the F10.7 and the climatology of the electron density distribution were used for internal assessment. It is found that the mean electron density is well correlated to the F10.7 index and that the distribution in electron density follows the well-known patterns in magnetic local time and magnetic latitude. The standard deviation of the binned values does show the largest variations in the equatorial regions and consequently the expected behaviour. For external validation, the corotating phase with Swarm B was assessed and an agreement within $10^{11} m^{-3}$ is derived. That level of agreement is also observed by radar measurements, whereas the radar measurements struggle from relatively large uncertainties at GRACE altitudes.